

2014-01-15

A Fast and Robust Image-Based Method for tracking Robot-assisted Needle Placement in Real-time MR Images

Satyanarayana Reddy Janga
Worcester Polytechnic Institute

Follow this and additional works at: <https://digitalcommons.wpi.edu/etd-theses>

Repository Citation

Janga, Satyanarayana Reddy, "A Fast and Robust Image-Based Method for tracking Robot-assisted Needle Placement in Real-time MR Images" (2014). *Masters Theses (All Theses, All Years)*. 106.
<https://digitalcommons.wpi.edu/etd-theses/106>

This thesis is brought to you for free and open access by [Digital WPI](#). It has been accepted for inclusion in Masters Theses (All Theses, All Years) by an authorized administrator of Digital WPI. For more information, please contact wpi-etd@wpi.edu.

A FAST AND ROBUST IMAGE-BASED METHOD FOR TRACKING ROBOT-ASSISTED
NEEDLE PLACEMENT IN REAL-TIME MR IMAGES

by

Satyanarayana Reddy Janga


A Thesis
Submitted to the Faculty
of the
WORCESTER POLYTECHNIC INSTITUTE
in partial fulfillment of the requirements for the
Degree of Master of Science
in
Computer Science

by

Satyanarayana Reddy Janga

July 2013

APPROVED:



Professor Michael Gennert, Major Advisor



Professor Gregory Fischer



Professor Eduardo Torres Jara

Abstract

This thesis deals with automatic localization and tracking of surgical tools such as needles in Magnetic Resonance Imaging(MRI). The accurate and precise localization of needles is very important for medical interventions such as biopsy, brachytherapy, anaesthesia and many other needle based percutaneous interventions. Needle tracking has to be really precise, because the target may reside adjacent to organs which are sensitive to injury. More over during the needle insertion, Magnetic Resonance Imaging(MRI) scan plane must be aligned such that needle is in the field of view (FOV) for surgeon. Many approaches were proposed for needle tracking and automatic MRI scan plane control over last decade that use external markers, but they are not able to account for possible needle bending. Significant amount of work has already been done by using the image based approaches for needle tracking in Image Guided Therapy (IGT) but the existing approaches for surgical robots under MRI guidance are purely based on imaging information; they are missing the important fact that, a lot of important information (for example, depth of insertion, entry point and angle of insertion) is available from the kinematic model of the robot. The existing approaches are also not considering the fact that the needle insertion results in a time sequence of images. So the information about needle positions from the images seen so far can be used to make an approximate estimate about the needle position in the subsequent images. During the course of this thesis we have investigated an image based approach for needle tracking in real-time MR images that leverages additional information available from robot's kinematics model, supplementing the acquired images. The proposed approach uses Standard Hough Transform(SHT) for needle detection in 2D MR image and uses Kalman Filter for tracking the needle over the sequence of images. We have demonstrated experimental validation of the method on Real MRI data using gel phantom and artificially created test images. The results proved that the proposed method can track the needle tip position with root mean squared error of 1.5 mm for straight needle and 2.5mm for curved needle.

Acknowledgements

I would like to express my deepest gratitude to my advisers: Dr. Michael Gennert and Dr. Gregory Fischer for their constant support and encouragement. Dr. Michael Gennert with his extensive knowledge, professional methodology and invaluable advice made a significant contribution to the quality of this work. I thank Dr. Gregory Fischer for his excellent guidance, caring, patience, and financially supporting my research. His technical expertise and visionary leadership in the field of medical robotics has significantly guided my research work and career development. Without his encouragement and effort this thesis would not have been completed.

Besides my advisers, I would like to thank Dr. Eduardo Torres-Jara for accepting the request as my thesis reader. I would like to express my sincerest gratitude to Computer Science Department for financially supporting my Masters study with Teaching Assistantship.

Furthermore, I would also like to thank my fellow labmates in Automation and Interventional Medicine Lab. Gang Li helped me with the experiments, Hao Su mentored me in the initial days, Nirav Patel for his help and suggestions with image processing concepts. In addition, I would like to thank Kevin Harrington, Wenzhi Ji, Yunzhao Ma, Hanlin Hong, Gregory Cole, Alex Camilo and Michael Delph for their help in many times.

I would like to express my gratefulness to my parents, my brothers and all my friends for their selfless love and encouragement. Lastly, most importantly I would like to thank my wife, Manjeera Dornala, for always being there cheering me up and stood by me through the good times and bad.

Contents

List of Figures	v
1 Introduction	1
1.1 Motivation and practical applications	1
1.2 MR Image Formation	3
1.3 Thesis Contribution	4
1.3.1 Problem Definition	4
1.3.2 Contribution	5
1.3.3 Thesis Organization	7
2 Previous Work	8
2.1 Standard Hough Transform	8
2.2 Variations of the Hough Transform	10
2.2.1 Analytic Hough Transform	10
2.2.2 Random Hough Transform	12
2.2.3 The Probabilistic Hough Transform	13
2.2.4 3D Hough Transform	14
2.3 RANSAC Model Fitting	14
2.4 Discussion	16
3 Needle Detection and Tracking	18
3.1 Needle Detection	19
3.1.1 SHT for Straight Needle Detection	20
3.1.2 Generalized Hough Transform for Curved Needle Detection	21
3.1.3 Tip Localization	22
3.2 Needle Tracking using Kalman Filter	22
3.3 Experiments & Results	25
3.3.1 Simulation Study	25
3.3.2 Experiments on real MRI data	37
3.4 Conclusion	41
4 Navigation Software	43
5 Future Work & Conclusions	48

Bibliography

List of Figures

1.1	MRI Hydrogen protons alignment	3
1.2	Overview of the Proposed approach	6
2.1	Image Space and Parameter Space for Hough Transform	9
2.2	Analytic Hough Transform Regions	11
3.1	Proposed Method	18
3.2	Needle Detection steps	19
3.3	Kalman Filter equations	23
3.4	Kalman Equations applied for needle tracking	24
3.5	Real MR prostate image	25
3.6	Algorithm for artificial image creation	26
3.7	Artificial images created for straight needle	27
3.8	Straight Needle tracking output	27
3.9	Error in tracking the ρ value for straight needle	28
3.10	Error in tracking the θ value for straight needle	29
3.11	Error in tip position tracking for straight needle	30
3.12	Time taken for needle tracking for Straight needle	31
3.13	Artificial images created for curved needle	32
3.14	Curved Needle tracking output	32
3.15	Error in tip position tracking for curved needle	33
3.16	Error in tracking the a value for curved needle	34
3.17	Error in tracking the b value for curved needle	35
3.18	Error in tracking the r value for curved needle	36
3.19	Time taken for needle tracking for curved needle	37
3.20	Needle tracking Gelatin images	38
3.21	Tracking a in Gelatin images	39
3.22	Tracking b in Gelatin images	40
3.23	Tracking r in Gelatin images	41
4.1	IGT Architecture	43
4.2	Data Visualization	44
4.3	Surgical Planning	45

4.4	Robot control software	46
4.5	Virtual Robot	47

Chapter 1

Introduction

Surgical instruments such as needles, electrodes and cannulas are inserted into the human body as part of minimally invasive surgical procedure [1]. Their location has to be known precisely and accurately during the interventions for correcting the possible needle bending and also for the Magnetic Resonance Imaging(MRI) scan-plane alignment, which is a motivation for our work(Section 1.1). Our goal is to develop an automatic localization and tracking method for needles in 2D MR images, by making use of the known information from robot kinematics model which helps in accurately navigating the surgical tool to the targeted location (Section 1.3). In the remaining part of this Chapter(Section 1.2) we introduce the reader to the principles and MR image formation.

1.1 Motivation and practical applications

Minimally Invasive Surgery (MIS) is one of the greatest advances in the history of surgery. It greatly reduces the patient's trauma compared to conventional open surgery by operating through natural body cavities and openings or small incisions into the body. It has been used tremendously in biopsy, brachytherapy seed placement and many other non-invasive application. During the procedure a surgical instrument, for example a needle or scissors is inserted into the body for seed placement or suturing. Since it is not possible to see the targeted tissue directly in needle based percutaneous procedures unlike open surgery, some form of medical imaging technology is used to assist the needle navigation. However, this

kind of surgical procedure requires a high amount of manual dexterity due to the complexities surrounded with MIS, which include lack of clear vision, instrument control inside the body and difficult hand-eye coordination [1]. To tackle these complexities and make the surgical procedure highly precise many surgical robots and visual aids are introduced. Surgical robotics systems were developed for image-guided neurosurgery, orthopedics, cardiac interventions, thoraco-abdominal interventions and prostate interventions. For movement-disorder surgery, the implantation of Deep Brain Simulator(DBS) has become increasingly popular. Cole, Wang and Fischer[2] [3] [4] developed and tested a MRI compatible robotic system for MRI-guided DBS electrode placement. Paul et al [5] developed a robot system for hip replacement guided by CT imaging. Rickers et al [6] employed real-time MRI to guide the placement of an atrial septal defect closure device. Xu et al proposed a robot system to assist lung biopsy using CT fluoroscopy images [7]. Fischer et al proposed a MRI-compatible robot system for transperineal prostate needle insertion using pneumatic actuation technique [8].

Image Guided Interventions Historically, physicians relied on their senses such as vision, touch and smell to diagnose illness, monitor a patient's condition, and perform invasive procedures. Last century has seen many innovations in imaging technologies such as X-ray, Ultrasound(US), Computed Tomography(CT), Sonar and Magnetic Resonance Imaging (MRI), which expose the areas of the body that would otherwise be impossible to see without using scalpel. Based on the significant growth in computing power and display capabilities over last couple of decades the surgical position can be simultaneously displayed on three dimensional orthogonal planes. Three-dimensional medical images are used not only for diagnosis, but also for planning the surgeries, thus evolved a concept referred to as image-guided interventions [1].

Typically Image Guided Interventions(IGI) has five sub-processes as described in [1]

1. Gather the preoperative images by any of the imaging techniques like X-rays,US, CT, MRI etc.
2. Localize and track the position of surgical tool.

3. Register the localizer volume with preoperative data.
4. Display the position of tool in preoperative data.
5. Account for differences between the preoperative data and intra-operative reality.

1.2 MR Image Formation

Having high spatial resolution, excellent soft tissue contrast and volumetric imaging capabilities, Magnetic Resonance Imaging (MRI) proves to be an effective imaging modality for image guided percutaneous interventions. MRI is based on the Nobel Prize winning phenomenon of “Nuclear Magnetic Resonance (NMR)”. NMR was first developed by Rabi et. al. [9] in 1938 and then it became a very powerful tool for chemical and physical molecular analysis. NMR is a phenomenon in which atomic nuclei, aligned in a magnetic field absorb and re-emit electromagnetic radiation. The frequency of energy, called resonance frequency is relative to the strength of the magnetic field and the magnetic properties of the isotopes of atoms. In the 1970s, Paul Lauterber [10], Richard Ernst [11] and Peter Mansfield [12] all independently showed the imaging potential of NMR and MRI was born [13].

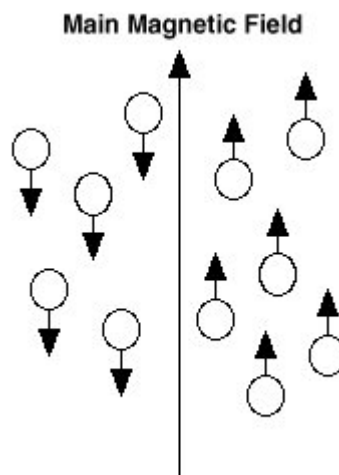


Figure 1.1: MRI Hydrogen protons alignment

MRI makes use of the fact that human body contains lots of water and fat, which contain many hydrogen nuclei or protons. When human body is placed inside the scanner, due to strong magnetic field all of the hydrogen protons will align with the magnetic field in one direction or the other as shown in Figure 1.1. These proton nuclei in tissues are raised to a higher state of energy when exposed to a short pulse of radiofrequency (RF) radiation. When the pulse is turned off, excited hydrogen protons emit RF energy as they return (relax) to their original energy state. During this relaxation a radio frequency signal is emitted which can be measured with receiver coils. To identify the spatial encoding of the signals, magnetic field is applied again which outputs the spatial origin of signal in 3D space by which 3D image can be formed[13].

1.3 Thesis Contribution

1.3.1 Problem Definition

The goal is to track needle position in MR imaging, it is accomplished through localization of needle segments in a time series of arbitrary 2d planes by making use of the additional information available from robot kinematics. As the needle is inserted, it might bend due to the resistance offered by tissue. So to make sure the needle accurately reaches the target, we need needle detection and tracking. Needle tracking is very important because some times the target might be adjacent to an organ which is sensitive to injury.

Challenges:- Since MRI is a can provide high resolution images, the amount of computation needed to identify the needle feature is very high. As the needle does not contain any hydrogen atoms, so there won't be any signal emitted and it leaves a noisy void artifact in the image. It gets even challenging if the image contains lot of bones, which are in similar intensity level as needle artifact.

Assumptions:- We are making following assumptions.

- 1) Needle bending will be little ($< 15^\circ$) from its actual path.
- 2) Needle artifact will be darker compared to the background.

- 3) Needle tracking is inherently 3D, but we are making the assumption that the needle falls in a arbitrarily oriented (oblique) 2D plane and we know that plane.
- 4) In the case of straight needle we are assuming that each 2D MR image contains a needle artifact and it will be straight.
- 5) In the case of curved needle we are assuming that each 2D MR image contains a needle artifact and it will be curved(i.e. a circular arc).

Output:- By making use of the available information(insertion point,insertion depth and direction of insertion)from robot kinematics model we would like to report the needle tip position and direction it is navigating to Scanner and robot. After receiving the information from needle tracking, Scanner aligns its scan plane and robot corrects the errors in its estimates of needle position.

1.3.2 Contribution

A fast and robust algorithm using Hough Transform is proposed for needle detection for both straight and curved needle. Since Needle insertion results in a time sequence of images, needle parameters detected from the current image can be used to make an approximate estimate for next image. So we proposed a real-time needle tracking algorithm using Kalman Filter, that can estimate the needle parameters for next image based on the observed parameters seen so far. It can also help in removing the possible outliers resulting from needle detection algorithm. Our proposed method also contains a robust tip localization method which uses parametrizing the needle in terms of insertion depth unlike many intensity based methods proposed[14] [15][16]. As shown in the Figure 1.2, our approach does the needle detection in closed loop with Scanner and Robot. We start by taking the initial estimates(entry insertion, direction of insertion, depth of insertion) from robot kinematics model and we receive realtime images from the MRI Scanner and apply needle detection method. For the subsequent steps we will take approximate estimates from Kalman Filter and insertion depth from robot kinematic model to assist in fast needle detection. At each step we report the needle position to robot, scanner and Kalman Filter

for updating their measurements.

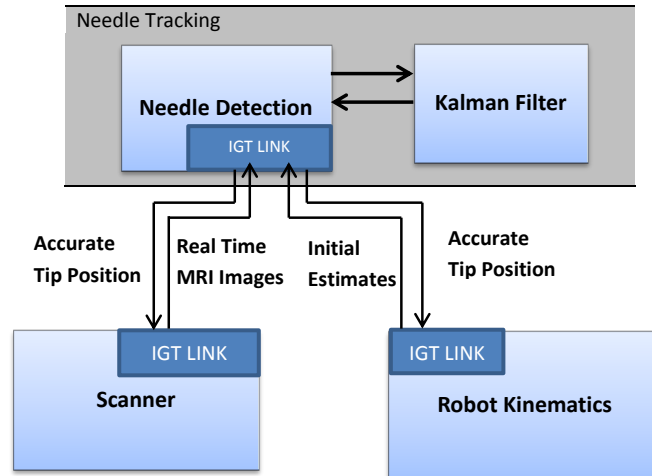


Figure 1.2: Overview of the Proposed approach

The proposed approach is tested on two types of data i) Simulated artificial prostate images ii) Real time MRI images taken during needle insertion into soft gelatin phantom. The results have shown that the proposed algorithm provides accurate estimations of needle parameters and tip's position.

As an advancement towards having a full fledged image guided surgical system, a Navigation Software that helps in path planning, visualization and surgical guidance is developed. The robot control software that send commands to the robot is integrated. Simulated visualization of the robot navigation is also implemented. The proposed needle tracking algorithms are integrated into our Navigation Software.

1.3.3 Thesis Organization

We review the previous approaches proposed for the surgical tool detection and tracking in Chapter 2. Our needle detection and tracking methods are described and results are discussed in detail in Chapter 3. In Chapter 4, we describe about the Navigation and surgical guidance Software developed for Image Guided Therapy(IGT) purposes. We conclude the thesis with a summary and future work in Chapter 5.

Chapter 2

Previous Work

Surgical tool localization is relatively new in the field of IGT using MRI but a great deal of work is already done for 2D/3D US. Most of the approaches proposed for US assume that the tool axis is straight and it appears bright in US image. For MRI, it is assumed that the object appears darker compared to the biological tissue.

A variety of algorithms are proposed for surgical tool detection in US and MRI. Standard Hough Transform(SHT) and its various modifications are widely used in US and MRI for straight needle detection are explained in Section 2.1 and Section 2.2. A model fitting approach using Random Consensus(RANSAC) is explained in Section 2.2. Discussion and Review of the tool localization methods is presented in Section 2.3.

2.1 Standard Hough Transform

Hough Transform is widely used feature detector in many image processing applications. Any shape that can be represented by a set of parameters can be detected using Hough Transform. It was first invented by Paul Hough in 1962 [17] and then later modified by Duda and Hart in 1972 [18]. Hough Transform follows the voting procedure, which is carried out in parameter space, from which shape candidates are obtained as local maxima in accumulator space that is constructed by the algorithm.

Hough Transform for Line Detection Line detection approach using SHT is used for identifying the needle. The most common line representation, known as the slope-intercept form, is $y = mx + b$ where m represents slope and b represents the Y-intercept. As shown in the Figure 2.1, each point (x_i, y_i) in image space represents a line in parameter space. Points lying on the same line in image space, define lines in the parameter space which all intersect at same point.

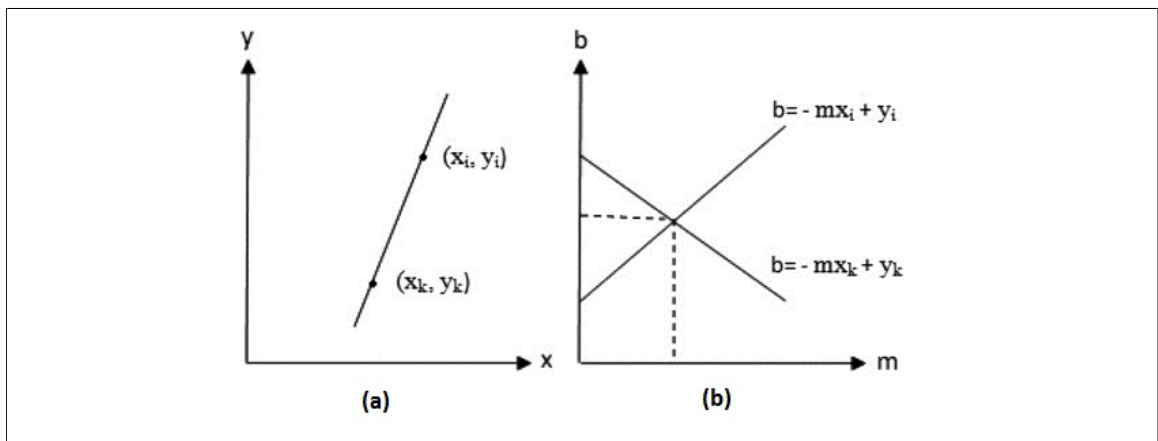


Figure 2.1: Image Space and Parameter Space for Hough Transform

The problem with slope-intercept form is limited that the slope, is unbounded for vertical lines need to be used two types of equations i.e. $y = mx + b$ for $-1 \leq m \leq 1$ and $x = ry + c$ for $-1 < r < 1$. An alternative linear function that does not have this limitation is the normal parametrization of a line, given by $\rho = x \cos \theta + y \sin \theta$, where ρ represents the perpendicular distance from the origin to the line and θ represents the angle of vector from origin to the closest point on the line in counter clock-wise direction with horizontal axis. When using the normal parametrization of a line it is standard that $\theta \in (0, 360]$ and ρ to be a non-negative value. Each point in image space represents a wave in parameter space. Points lying on the same line in image space, define waves in the parameter space which all intersect at same point in parameter space. As shown in the Algorithm 1 parameter space is discretized into accumulator bins. The bins with the peaks represent the line candidates.

```

initialization  $Acc[\rho_{min}..\rho_{max}][\theta_{min}..\theta_{max}] = 0$  ;
for each edge point  $(x, y)$  do
    for  $\theta = \theta_{min}; \theta \leq \theta_{max}; \theta ++$  do
         $\rho = x \cos(\theta) + y \sin(\theta)$ ;
         $Acc[\rho][\theta] ++$ ;
    end
end
Find local maxima  $Acc[\rho][\theta]$ ;

```

Algorithm 1: Standard Hough Transform Algorithm

The complexity of the SHT Algorithm increases with the increase in the granularity of discretization. It is also generalized for detecting other shapes [19], e.g. circle, ellipse. The computational complexity increases exponentially with the number of parameters for representing the shape.

2.2 Variations of the Hough Transform

Many modifications of SHT are proposed in the literature for optimizing the computational complexity and accuracy of feature detection. Some of them are reviewed in this section.

2.2.1 Analytic Hough Transform

The Analytic Hough Transform(AHT) is an extension of SHT, which can produce the results of features upto sub-pixel accuracy. Unlike SHT it does not use voting procedure in parameter space. It treats each pixel as a region so there can be many lines that pass through two pixels, where as in SHT, there exists only one line that passes through two given pixels. It extends the traditional Slope-Intercept form ($y = m * x + b$) by avoiding the problems with slope reaching infinite, using the inverse of slope(r) for that interval. For

each edge pixel the algorithm creates four Analytic Hough Regions(AHR), which exactly represents the set of all lines through a pixel as shown in Figure 2.2.

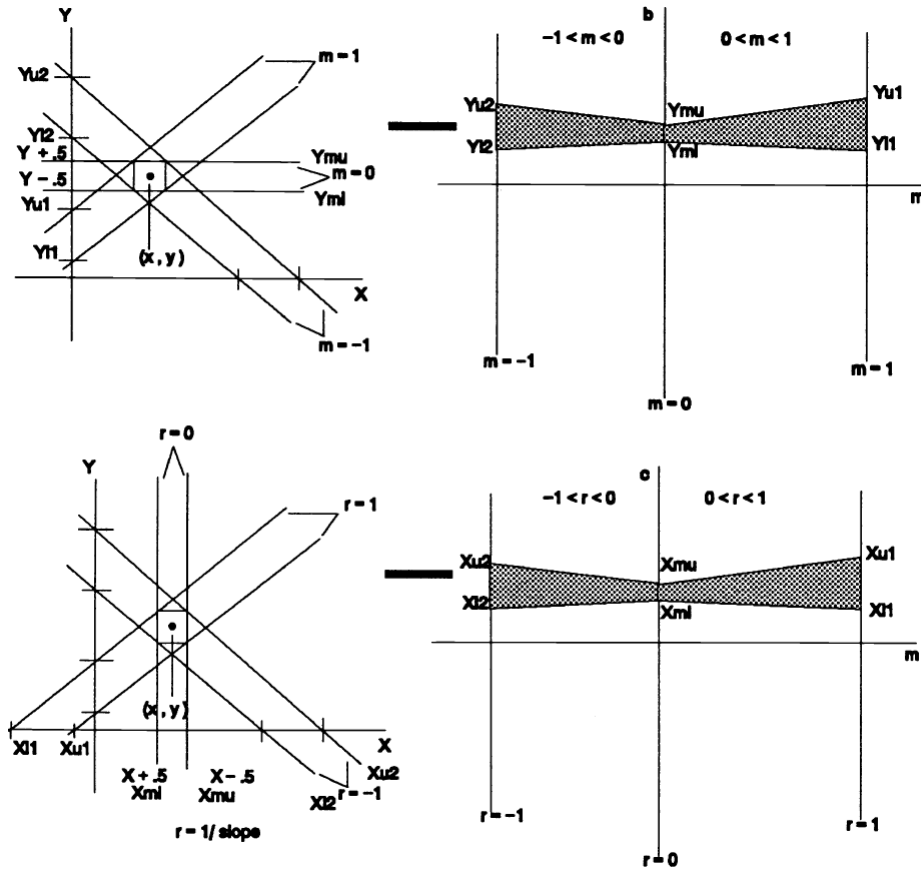


Figure 2.2: The four analytic regions formed for each pixel (x, y) [20]

```

initialization;;
AHR1 < Region, count >:= nil;
AHR2 < Region, count >:= nil;
AHR3 < Region, count >:= nil;
AHR4 < Region, count >:= nil ;
for each edge pixel (x,y) do
  for i = 1 to 4 do
    Regioni = create ith analytic region for (x,y);
    for each Region in AHR do
      if Regioni intersects with Region then
        count = AHRi.get(Region);
        AHRi.remove(Region);
        AHRi.add(Regioni - Region, 1);
        AHRi.add(Region ∩ Regioni, count + 1);
        AHRi.add(Region - Regioni, count);
      end
    end
  end
end
end
Find Region with max Count

```

Algorithm 2: AHT Algorithm

As explained in Algorithm 2, after analyzing the regions for each pixel, the numbers of regions increases and also the count for each region that analyzes the pixel. In the end the region with maximum count represents the feature lines formed with the given pixels.

2.2.2 Random Hough Transform

The Randomized Hough Transform follows a non-deterministic voting procedure. It has been proposed by Xu et. al.[21][22][23]. The RHT Algorithm 3 iteratively selects random

pairs of points from input pixels and updates the accumulator bins in the Hough space. After running sufficient number of iterations, local maxima from accumulator are selected as candidates for line object.

```

initialization  $Acc[\rho_{min}.. \rho_{max}][\theta_{min}.. \theta_{max}] = 0$  ;
 $N :=$  number of iterations ;
 $i = 0$  ;
while  $i < N$  do
    |   Select random pair of points  $(x_1, y_1), (x_2, y_2)$  from the edge points;
    |   Compute  $(\rho, \theta)$  from the selected pair of points;
    |    $A[\rho, \theta] ++$ ;
    |    $i ++$ ;
end
Find local maxima  $Acc[\rho][\theta]$ ;

```

Algorithm 3: Random Hough Transform Algorithm

It is computationally less expensive because in each iteration only one accumulator bin is incremented unlike Standard Hough Transform. We can increase the granularity of accumulator space with out any computation overhead. It works exceptionally well for low noise, high quality images. Later it has been extended to 3D line detection [24].

2.2.3 The Probabilistic Hough Transform

Kiryati et al [25] described an algorithm which is very similar to SHT. The difference from SHT is that rather than using all the N edge points, only a subset n is used. As $n \ll N$, the complexity of the voting stage is reduced. This works because a random subset of N will fairly represent all features and noise based on the area they occupy in the image. The value of n must be chosen carefully such that it should not be too small and not too big.

Kiryati et al performed an analysis and suggested value for n to be 2 – 5% of N .

2.2.4 3D Hough Transform

The Standard Hough Transform is generalized to detect lines in 3D space [26] [27][24]. The line in 3D passing through point p and vector v is defined with the spherical coordinates as below [28]:

$$L_{\phi,\rho,\theta,r} : [x(t), y(t), z(t)] = p_{\theta,\rho} + tv_{\phi,\rho} \quad (2.1)$$

$$p_{\theta,r} = [r \cos(\theta), r \sin(\theta), 0] \quad (2.2)$$

$$v_{\phi,\rho} = [\cos(\phi) \cos(\rho), \sin(\phi) \cos(\rho), \sin(\rho)] \quad (2.3)$$

where point $p_{\theta,\rho}$ is an intersection of line with base plane (intercept point with the plane xy). In 3D case the Hough space is 4D accumulator so the line detection is very computationally complex.

Bhattacharya et al. [29] developed a fast version of Standard 3D Hough Transform called (2+2)D Hough Transform.

They decompose the line detection in 3D into:

- (i) finding the slope of 3D line in 2D parameter space (ϕ, ρ)
- (ii) finding its intercept $p_{\theta,\rho}$ of a 3D line also in 2D parameter space.

The demonstrated experimental results on different variety of 3D images shown to be significantly fast compared to Standard 3D Hough Transform.

2.3 RANSAC Model Fitting

The RANSAC is a non-deterministic iterative method to estimate parameters of a mathematical model from a set of observed data which contains outliers. The procedure was introduced by Fischler and Bolles in 1981 [30]. In the case of needle detection the input is a set of thresholded voxels V from 3D US and a probabilistic function that makes the distinction between inliers and outliers. In each iteration of Algorithm 4, model is built by selecting a random sample from the data points. The model is evaluated with all data points and error is calculated. If it is better than the already selected best model, current model is marked as best seen so far.

```

Input:
 $P$  := Input voxels;
 $f$  := classification function;
Output:
best_model := model parameters which best fit the data;
best_consensus_set := data points from which this model has been estimated;
best_error := the error of this model relative to the data;
 $i = 0$  ;
while  $i < I_{max}$  do
    maybe_inliers := n randomly selected values from data;
    maybe_model := model parameters fitted to maybe_inliers;
    consensus_set := maybe_inliers;
    for each point  $p$  in  $P$  do
        if  $f(p)$  then
            add point to consensus_set ;
        end
    end
    if  $|consensus\_set| > d$  then
        this_model := model parameters fitted to all points in consensus_set ;
        this_error := error in the model fitted to consensus_set;
        if  $this\_error < best\_error$  then
            best_model := this_model;
            best_consensus_set := consensus_set;
            best_error := this_error;
        end
         $i = i + 1$ ;
    end
end
return best_model, best_consensus_set, best_error ;

```

Algorithm 4: RANSAC Algorithm

2.4 Discussion

Roland et. al. [16] uses a 2D MR image incident with a needle to track the biopsy needle in prostate. They proposed a SHT based straight needle tracking algorithm for enabling the automatic MRI scan-plane alignment. For optimizing the computational complexity associated with SHT they used reduced field of view 2D MRI, which may not always be the case. Their approach will not extend to the case of curved needles. The needle tip localization method employed is not robust because the noisy artifact might not visible in the image, Moreover the image processing steps applied (dilation,erosion and thinning) might erode the tip position.

Ding et. al. [14] [15] developed Hough Transform based methods for needle segmentation. They optimized the algorithm by using 2D projections of 3D US. The proposed methods are for linear feature detection and they do not extend for curved tool detection. Okazawa et. al. [31] proposed a two-step method to segment surgical tool of constant curvature based on Hough Transform. In the first step they approximate the estimate for needle axis based on edge-detection like method applied in different directions. In the second step they apply Generalized Hough Transform for curved needle detection. But the algorithm did not propose any tip localization methods and the direction of needle movement at the tip position.

Uhercik et. al. [32] and Ren et. al. [33] proposed robust RANSAC based model fitting for the surgical tool, defined by a set of parameters. In both of these methods the image is pre-processed and thresholded to reduce the amount of data used for model fitting. The model fitting algorithms were applied for object detection of different shapes. Since RANSAC tries to fit as many inliers as possible, the object detection might fail on the real MRI data because generally the number of background pixels will be more than the number of foreground pixels. Moreover RANSAC is a non-deterministic algorithm, it has to run sufficient number of iterations to get the best model, which needs to be set for case to case.

The AHT algorithm [20] proposed for line detection proved to give the sub-pixel level accurate results. The run time complexity of the algorithm is very high that the number of analytic regions increase exponentially with the number of pixels. So it is not feasible for the needle detection in MRI as the number of pixels to be considered for feature detection are very high. So the SHT based approaches are faster for feature detection in MRI compared to AHT.

Chapter 3

Needle Detection and Tracking

The proposed needle tracking algorithm runs the following two steps at each timepoint of needle insertion in a closed loop as shown in Figure 3.1. i) Taking the information from Robot and Kalman Filter and detect the needle in a 2D MR image. ii) Updating the estimates of Kalman Filter based on needle detection output.

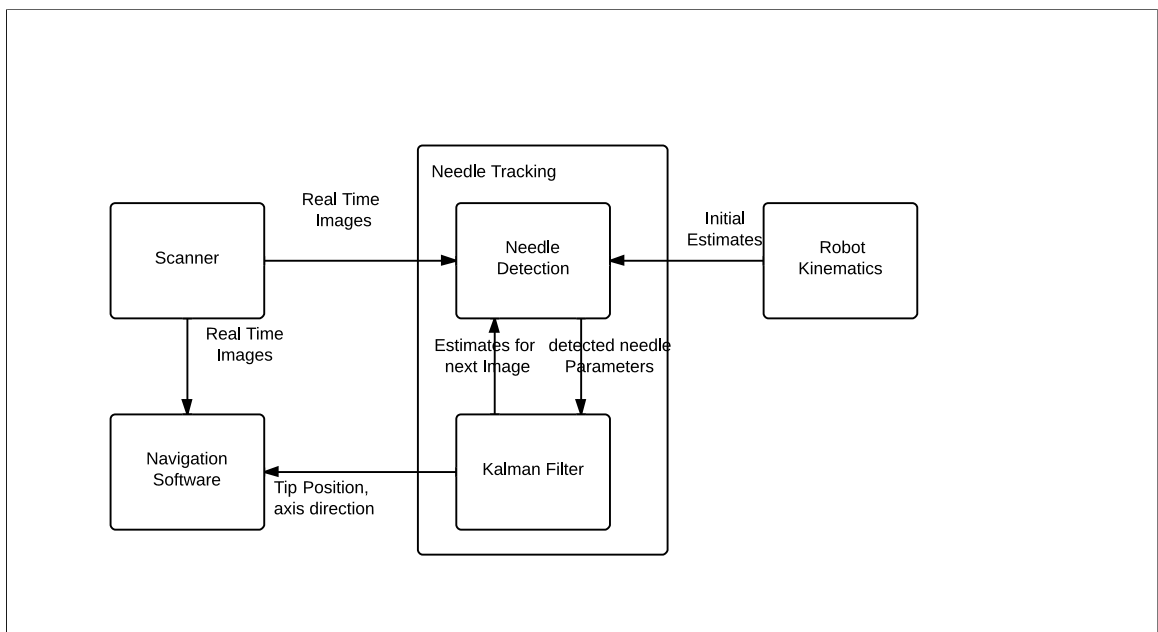


Figure 3.1: Needle Detection in Closed loop with Kalman Filter

3.1 Needle Detection

MRI has proven to be a versatile non-invasive imaging technique for IGT purposes. As the needle does not contain any hydrogen atoms, MRI does not get any signal and it creates a noisy void artifact in the MR image, which makes it very tough for the segmentation. It gets even challenging if the surgical region contains bones which are at the same intensity level as the needle artifact. As shown in the Figure 3.2, we follow a series of steps to identify the needle information and report it back to the navigation software.

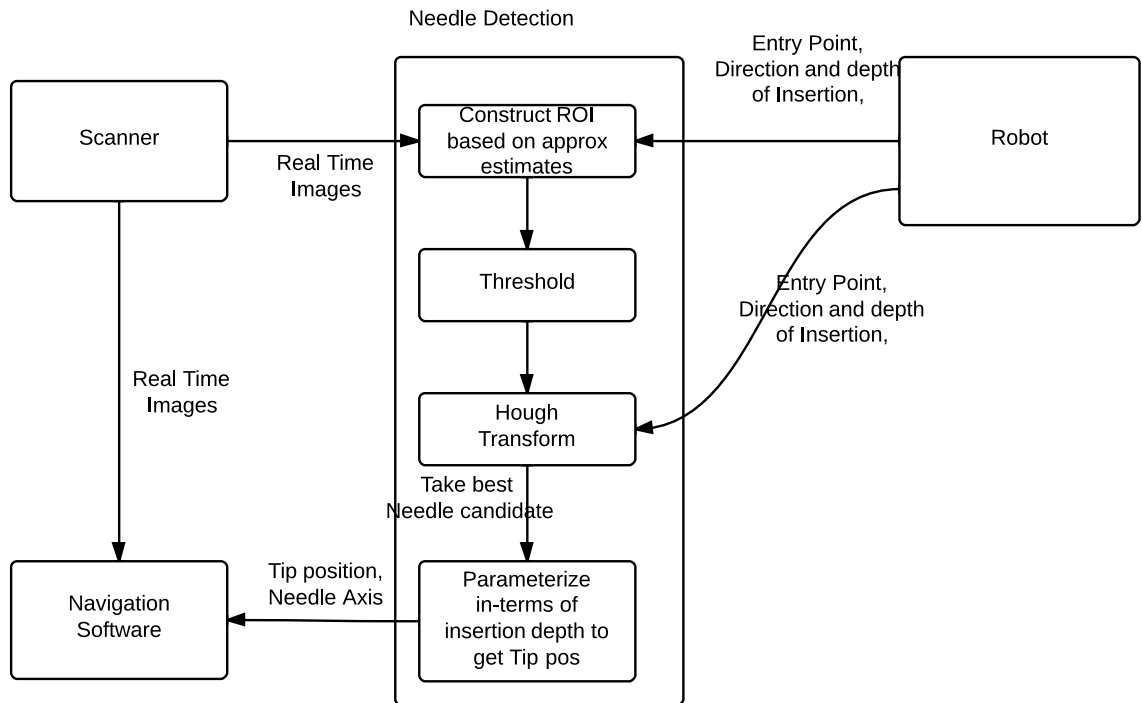


Figure 3.2: Needle Detection flow and the series of steps applied to the image

- 1) **Take the real time MR images from scanner :-** Receive the real time images by using the communication protocol OpenIGTLink [34]
- 2) **Construct the Region of Interest(ROI) :-** We use entry position, direction and depth of insertion coming from the robot kinematics model to create ROI in the first few

images. In the later steps we use the estimates from Kalman Filter along with the insertion depth from robot kinematics model to create the ROI for the needle.

3) Thresholding:- We threshold the image based on the intensity range for the needle. As MRI does not get any signal from needle, the needle will be a dark artifact. So a low intensity value (< 50) is used as threshold.

4)Hough Transform:- We apply Hough Transform to identify the best candidate for the needle object. Constructing ROI significantly decreases the computation complexity of Hough Transform. Also as we know the approximate estimates for the needle shape feature, we can create more coarser hough bins to make the needle detection highly precise. We are using the SHT for straight needle detection(Section 4.1.1)and Generalized Hough Transform (Section 4.1.2)for curved needle detection.

5)Parametrise the needle in-terms of insertion depth(l):- Since we would like to know tip position, we parametrize the needle with its insertion depth ($X(s), Y(s)$) such that the entry position is at $s = 0$. So the tip position will be at $s = l$. By this way we can identify the tip position and needle navigation direction precisely (Section 3.1.3).

3.1.1 SHT for Straight Needle Detection

Line detection using SHT can be employed for straight needle detection as explained in Section 2.2. During the initial steps of needle insertion, we use entry position, direction and depth of insertion coming from the robot kinematics model to create approximate estimate for needle parameters (ρ, θ) and in the later steps Kalman Filter gives the estimate for needle parameters (ρ, θ) .

Based on the assumptions we made, the needle bending will be $< 15^\circ$ from its actual path, the value for $\Delta\theta$ is 15° . The $\Delta\rho$ is set as a factor(= 20) of needle thickness and pixel spacing in the image. With this information we can construct very coarser bins for the SHT within the range $(\rho \pm \Delta\rho, \theta \pm \Delta\theta)$ and can still get the output in real time.

3.1.2 Generalized Hough Transform for Curved Needle Detection

For identifying the curved needle Generalized Hough Transform is used. As we know the circle representation of equations

$$x = a + r \cos \theta \quad (3.1)$$

$$y = a + r \sin \theta \quad (3.2)$$

where (a, b) represent the center of the arc and r represents the radius of curvature $[0, \infty)$ and $\theta \in (0, 360^\circ]$.

```

initialization  $Acc[b_{min}..b_{max}][b_{min}..b_{max}][r_{min}..r_{max}] = 0$  ;
for each edge point  $(x, y)$  ; do
    for  $r = r_{min}; r \leq r_{max}; r ++$ ; do
        for  $\theta = 0; \theta < 360; \theta ++$ ; do
             $a = x - r \cos \theta$ ;
             $b = y - r \sin \theta$ ;
             $Acc[a][b][r] ++$ ;
        end
    end
end
Find local maxima  $Acc[a][b][r]$ ;

```

Algorithm 5: Generalized Hough Transform Algorithm for Circle Detection

During the initial steps of needle insertion, we use entry position, direction and depth of insertion and approximate radius of curvature coming from the robot kinematics model to create approximate estimate for needle parameters (a, b, r) and in the later steps Kalman Filter gives the estimate for needle parameters (a, b, r) .

Based on the assumptions we made, the needle deviation is little from its actual path, the value for Δr is used as 10% of r . The Δa and Δb is set as a factor(=20) of needle thickness

and pixel spacing in the image. With this information we can construct very coarser bins for the GHT with in the range $(a \pm \Delta a, b \pm \Delta b, r \pm \Delta r)$ and can get the output in real time.

3.1.3 Tip Localization

Identifying tip position and the direction of needle navigation is challenging because the noisy needle artifact incident on the image might not even contain the tip in it. To know the tip position, we are parametrizing the needle with its insertion depth $(X(s), Y(s))$, such that the entry position is at $s=0$ then the tip position will be at $s = l$, where l is insertion depth. By this way we can identify the tip position and direction of needle navigation precisely. This parametrization also helps to look ahead and confirm whether the needle is going in the direction of target. The following are the parametrization equations for straight needle.

$$X_s = X_0 + s * \cos(\alpha) \quad (3.3)$$

$$Y_s = Y_0 + s * \sin(\alpha) \quad (3.4)$$

where (X_0, Y_0) is entry point taken from Kinematics Model, (X_l, Y_l) is the needle tip position after inserting length l and α is slope angle of the line calculated from needle parameters ρ and θ .

These are the parametrization equations for curved needle.

$$X_s = a + r * \cos(\alpha) \quad (3.5)$$

$$Y_s = b + r * \sin(\alpha) \quad (3.6)$$

where (a, b) is the center of the circular arc, r is the radius and $\alpha =$ angle formed by arc calculated by using l/r .

3.2 Needle Tracking using Kalman Filter

Since MRI is a time sequence imaging and the amount of needle insertion between the adjacent images in the sequence is less. By using Kalman Filter, the needle parameters from the images seen so far can be used to make an approximate estimate for the needle parameters in the next image .

Kalman Filter:- Kalman Filter is a widely used probabilistic filter in many navigation and tracking applications, which was invented by R.E. Kalman in 1960 [35]. It is a set of mathematical equations which recursively estimates the underlying state of the system by taking the series of measurements observed over time, containing noise and other inaccuracies. It makes the assumptions that the system is a linear Gaussian system.

Linear state transition: $x_t = A_t x_{t-1} + B_t u_t + \epsilon_t$

where A_t, B_t are the state transition matrices u_t is the control vector and ϵ_t is the additive Gaussian noise

Linear measurement model: $z_t = H_t x_t + \delta_t$

where H_t is the measurement matrix that relates the state x_t to the measurement z_t and δ_t is additive Gaussian noise

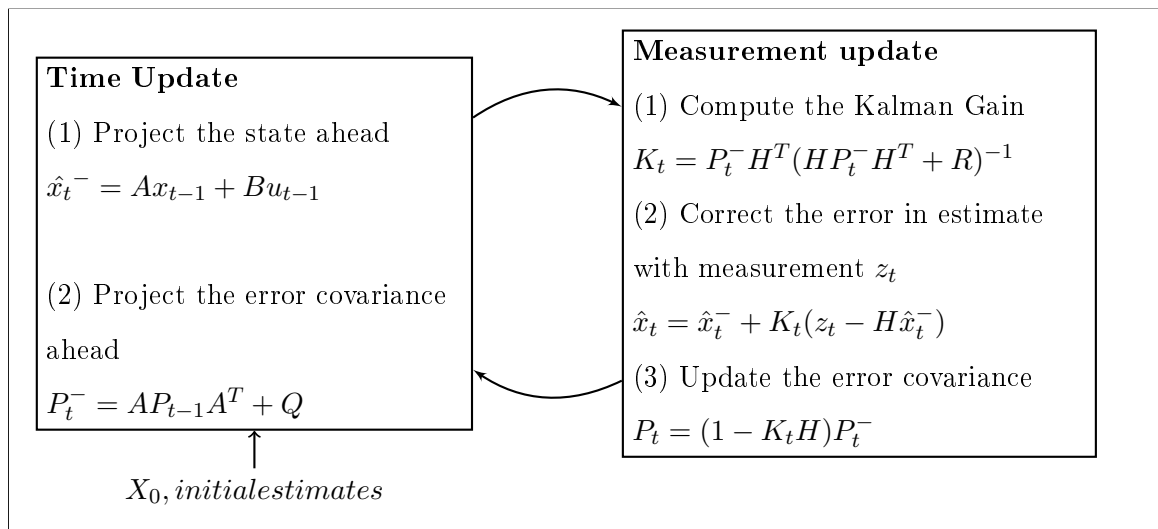


Figure 3.3: Kalman Filter :- estimate and measurement update equations

Figure 3.3 shows the estimate and measurement update equations for Kalman Filter(KF). X_0 is the initial state estimate, K_t is the Kalman Gain, P_t is estimation error co-variance, Q & R are process and measurement noise co-variances.

KF for needle tracking:- Figure 3.4 shows the KF equations we used for tracking the needle parameters for both curved and straight needles.

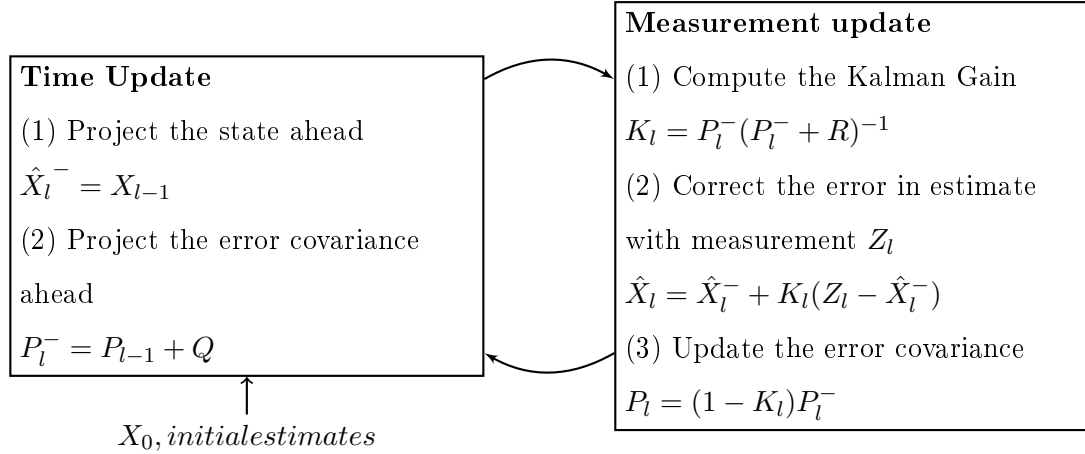


Figure 3.4: Kalman Filter Needle Tracking Equations. Both state estimate and measurement update equations for the needle parameters.

The state and noise co-variance matrices for tracking the straight needle are as shown below.

$$X_l = \begin{pmatrix} \rho_l & 0 \\ 0 & \theta_l \end{pmatrix}; P_l = \begin{pmatrix} P_{\rho_l} & 0 \\ 0 & P_{\theta_l} \end{pmatrix}; Q = \begin{pmatrix} Q_{\rho} & 0 \\ 0 & Q_{\theta} \end{pmatrix}; R = \begin{pmatrix} R_{\rho} & 0 \\ 0 & R_{\theta} \end{pmatrix}$$

The state initialization is done by taking the random parameters from the range ($\rho \pm \Delta\rho, \theta \pm \Delta\theta$) created by taking the initial estimates from kinematics model.

The state and noise co-variance matrices for tracking the curved needle are as shown below.

$$X_l = \begin{pmatrix} a_l & 0 & 0 \\ 0 & b_l & 0 \\ 0 & 0 & r_l \end{pmatrix}; P_l = \begin{pmatrix} P_{a_l} & 0 & 0 \\ 0 & P_{b_l} & 0 \\ 0 & 0 & P_{r_l} \end{pmatrix}; Q = \begin{pmatrix} Q_a & 0 & 0 \\ 0 & Q_b & 0 \\ 0 & 0 & Q_r \end{pmatrix}; R = \begin{pmatrix} R_a & 0 & 0 \\ 0 & R_b & 0 \\ 0 & 0 & R_r \end{pmatrix}$$

The state initialization is done by taking the random parameters from the range ($a \pm \Delta a, b \pm \Delta b, r \pm \Delta r$) created by taking the initial estimates from kinematics model.

Implementation Details ImageJ(<http://rsbweb.nih.gov/ij/>) is used for loading the Dicom images and applying the image processing filters. Hough Transform algorithms and Kalman Filter are implemented in Java. All the implementations were performed on a personal computer (Dell OPTIPLEX 7010, CPU: Intel Core i5 (64 bit)3.30GHz GHz, Memory: 4 GB, OS: Ubuntu 12.10, Dell Inc., Round Rock, TX). The proposed approaches are integrated into Navigation Software (Chapter 4).

3.3 Experiments & Results

We validated our methods by experimenting over two different types of data collected.

3.3.1 Simulation Study

Many simulated images of straight and curved needles were created by artificially painting a noisy needle of 1.41mm diameter over a real time prostate MR image of resolution 576x584 and with pixel spacing of 0.352mm as shown in Figure 3.5(Images are taken from our collaborators at Brigham and Women’s Hospital).

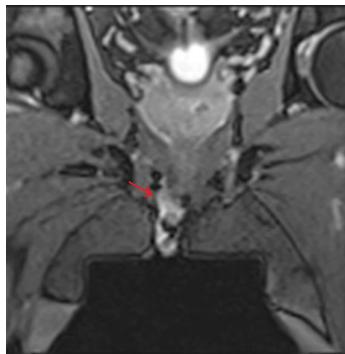


Figure 3.5: Base image used for generating simulated needle images

Image Creation:- We created many artificial needle images which resembles to the MR images for prostate purposes. Figure 3.5 shows an example of a real MR images captured for straight needle insertions. We can observe that the needle artifact is not clearly visible

and also breaks at many points. To create such a representation for the artificial image we followed the algorithm displayed in Figure 3.6.

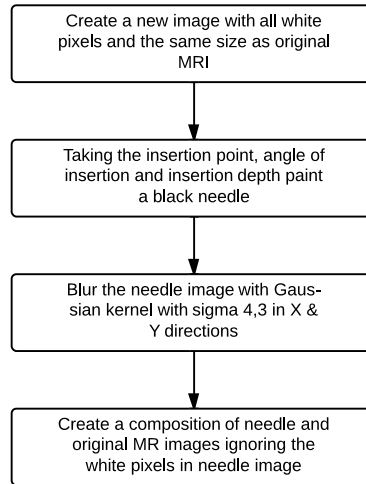


Figure 3.6: Algorithm for artificial image creation

Straight Needle We have artificially generated a series of 220 needle images with increasing insertion depth of 1 pixel distance(0.352mm) for each image by using Algorithm in Figure 3.6. Some of the images created are shown in Figure 3.7. Since we know the ground truth values for insertion depth, direction of insertion and needle position in each image, we compared these values against the results obtained through the proposed method.

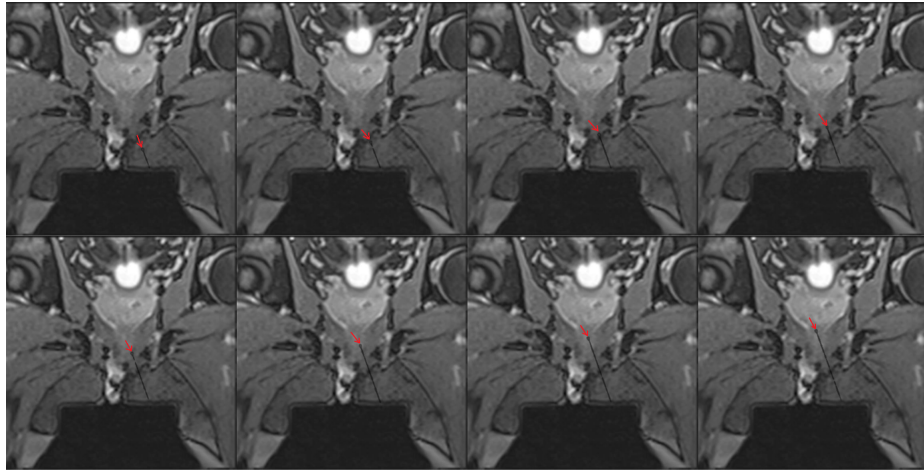


Figure 3.7: Some of the many simulated straight needle images used for simulation study

Figure 3.8 contains the Original image, Thresholded image based on the needle intensity range and Output of the needle tracking. The needle painted in the green represents the approximate estimate and blue represents the needle detection output and red represents corrected estimate value based on needle detection output.

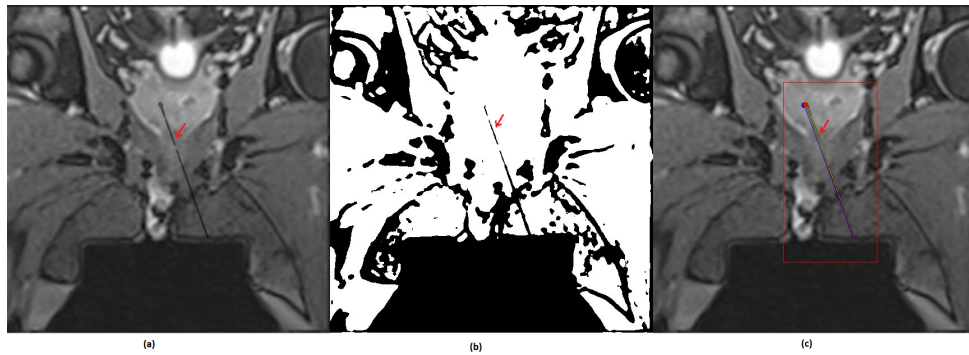


Figure 3.8: a) Original needle Image b) Threshold image c) Needle detection output for straight needle

Figure 3.9 shows the deviation of detected and tracked values of ρ from actual needle parameters. The values represented in red are needle detection output and the values represented in blue are output from KF tracking. We can see that the tracked value of ρ is converging close to zero.

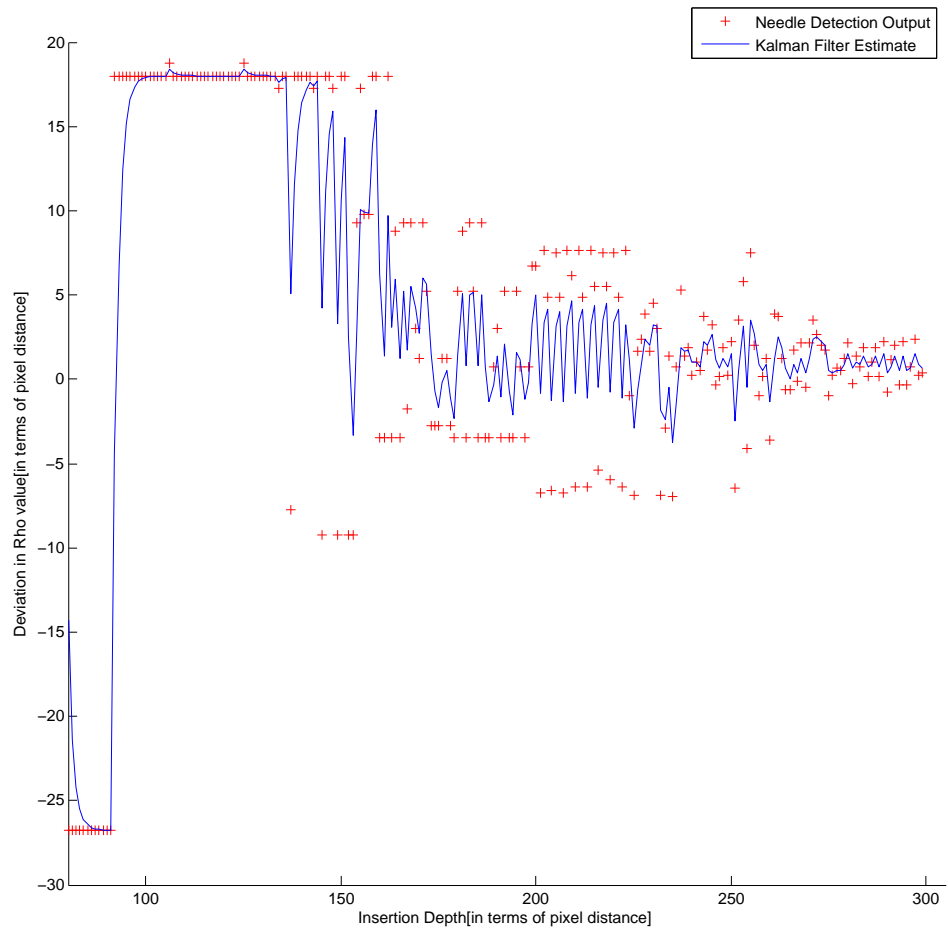


Figure 3.9: Deviation in ρ value in needle detection output and KF tracking from actual needle parameters for straight needle tracking. In the image the pixel spacing is 0.352mm

Figure 3.10 shows the deviation of detected and tracked values of θ from actual needle parameters. The values represented in red are detected output from needle and the values represented in blue are output from KF tracking. We can see that the tracked value of θ is converging close to zero.

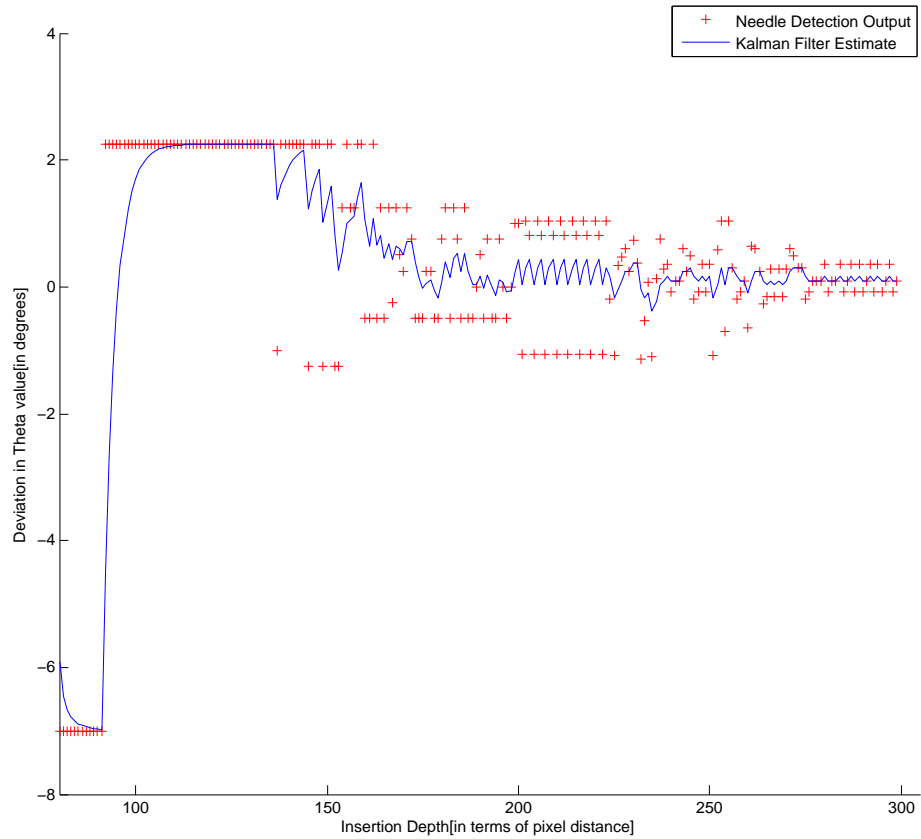


Figure 3.10: Deviation in θ value in needle detection output and KF tracking from actual needle parameters for straight needle tracking. In the image the pixel spacing is 0.352mm

Figure 3.11 shows the deviation of X vs Y from actual values of tip position. The values represented in blue are detected output from needle and the values represented in red are output from KF tracking.

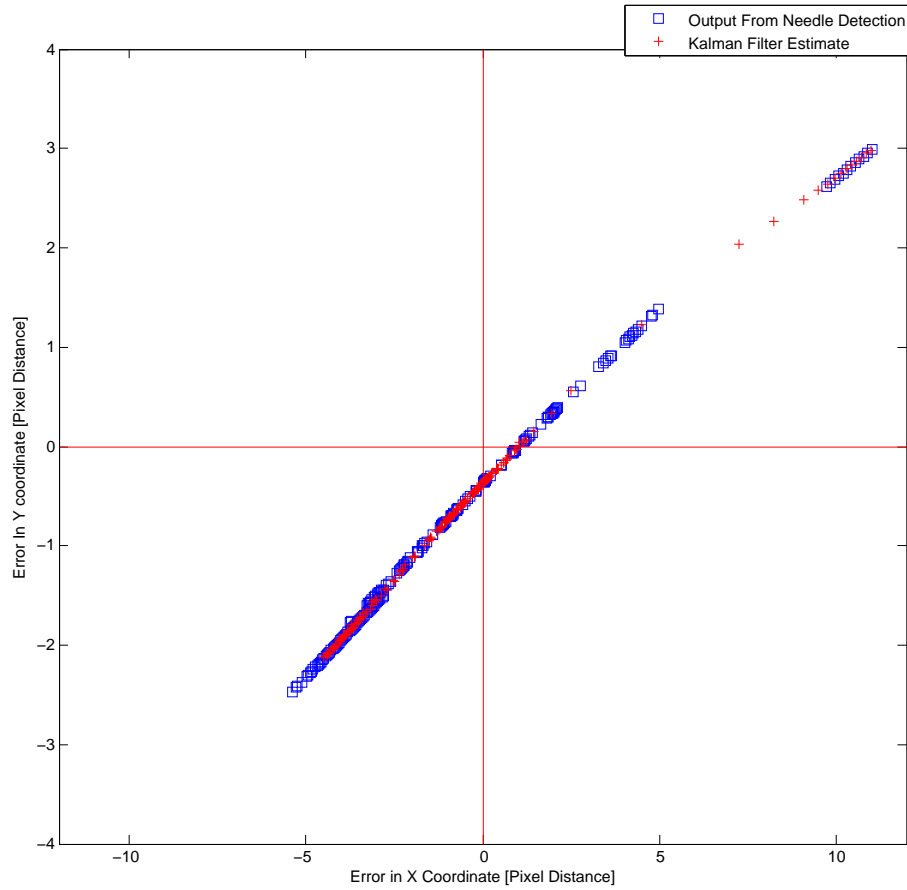


Figure 3.11: Deviation in tool tip position in needle detection output and KF tracking from actual needle parameters for straight needle tracking. In the image the pixel spacing is 0.352mm

Figure 3.12 shows the time taken for needle tracking in each image. We can see that algorithm running time is increasing with the insertion depth because ROI also increases with insertion depth. Overall the algorithm runs less than 0.25s.

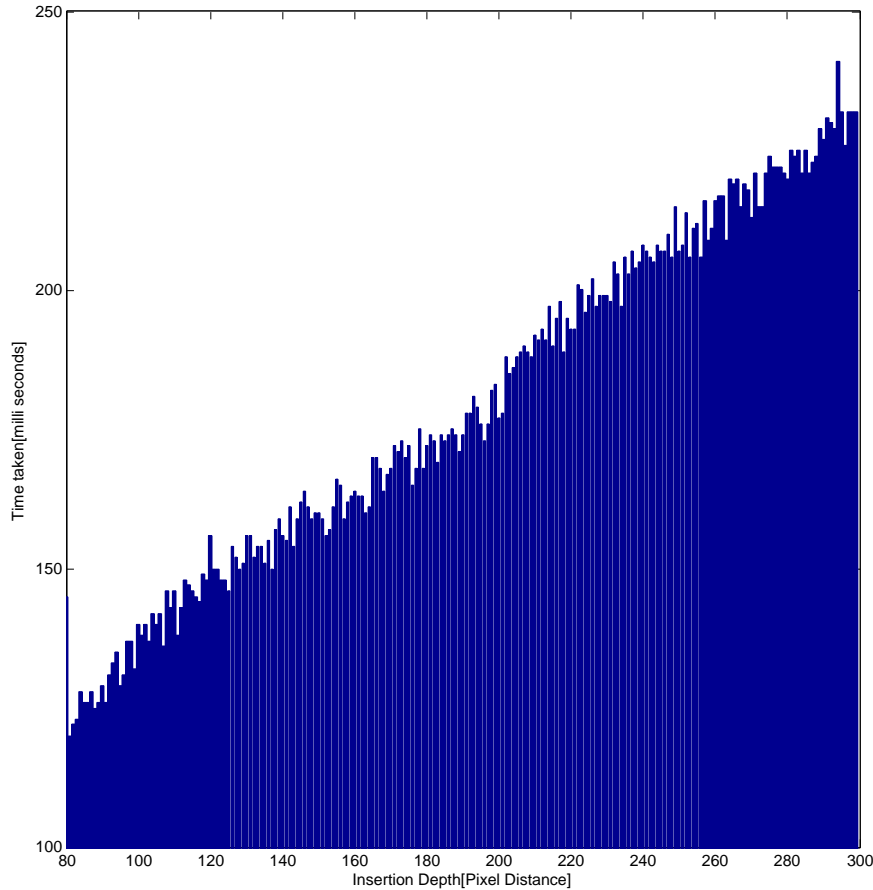


Figure 3.12: The time taken for needle tracking in the straight needle images

Curved Needle We have generated a data set mimicking a curved needle insertion into prostate. We have artificially generated a series of 220 needle images with increasing insertion depth of 1 pixel distance (0.352mm) for each image by using Algorithm in Figure 3.6. Some of the examples images are shown in Figure 3.13. Since we know the exact values of depth of insertion, direction of insertion, radius of curvature and needle position in each image, we compared these values against the results obtained through our method.

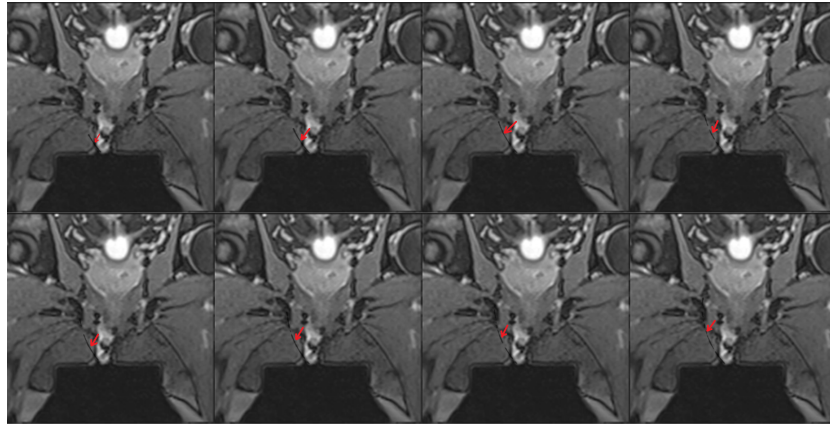


Figure 3.13: Some of the many simulated curved needle images used for simulation study

Figure 3.14 contains the Original image, Thresholded image based on the needle intensity range and Output of the needle tracking. The needle painted in the green represents the approximate estimate and blue represents the needle detection output and red represents corrected estimate value based on needle detection output.

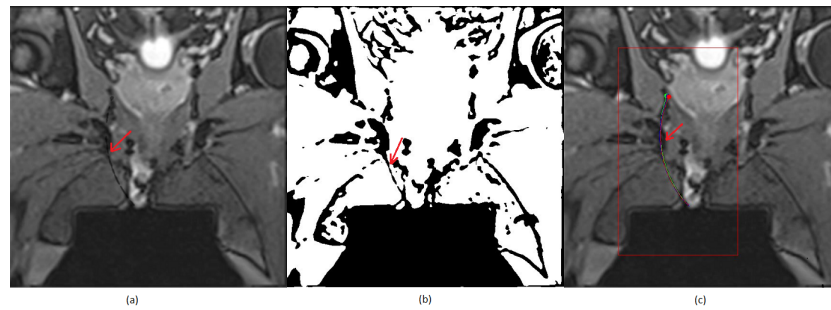


Figure 3.14: a) Original needle Image b) Threshold image c) Needle detection output for Curved needle

Figure 3.15 shows the deviation of X vs Y from actual values of tip position. The values represented in blue are detected output from needle and the values represented in red are output from KF tracking.

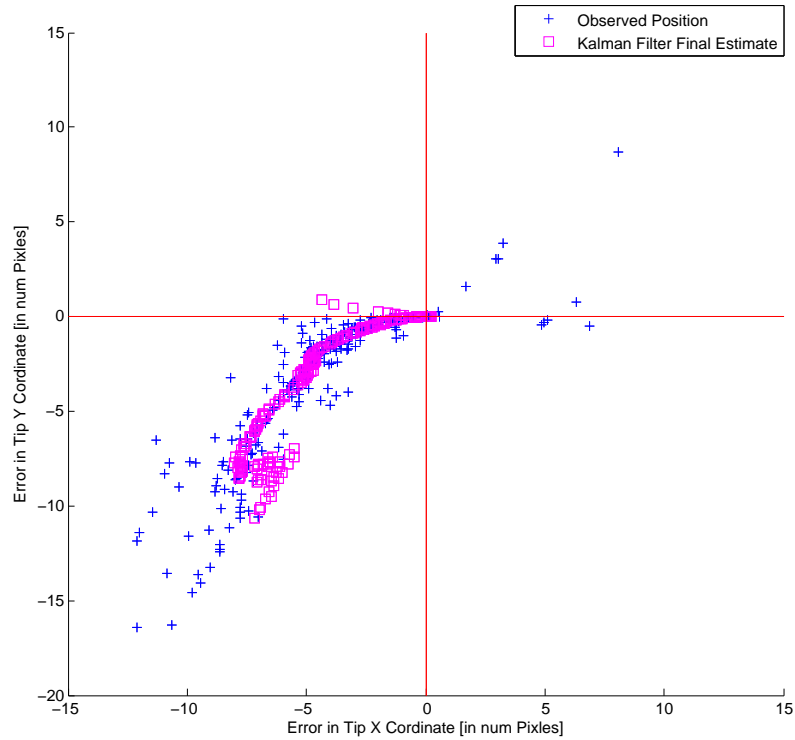


Figure 3.15: Deviation in tool tip position in needle detection output and KF tracking from actual needle parameters for curved needle tracking. In the image the pixel spacing is 0.352mm

Figure 3.16 shows the deviation of detected and tracked values of X coordinate of the center of arc (a) from actual needle parameters. The values represented in red are detected output from needle and the values represented in blue are output from KF tracking.

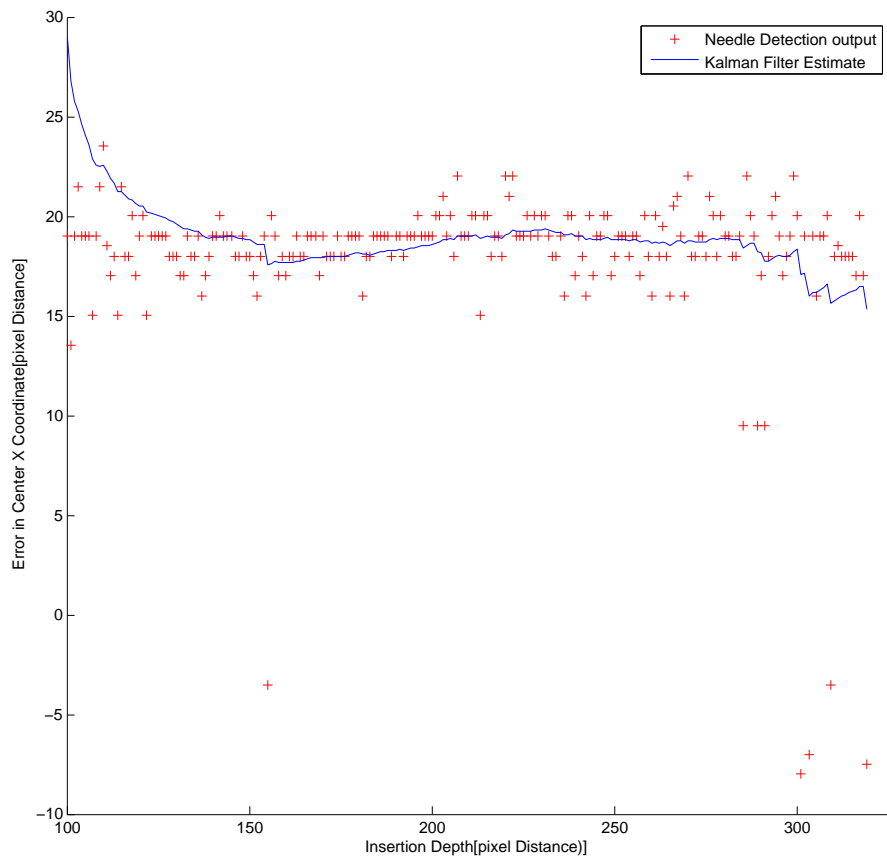


Figure 3.16: Deviation in center X coordinate(a) in needle detection output and KF tracking from actual needle parameters for curved needle tracking. In the image the pixel spacing is 0.352mm

Figure 3.17 shows the deviation of detected and tracked values of Y coordinate of the center of arc (b) from actual needle parameters. The values represented in red are detected output from needle and the values represented in blue are output from KF tracking.

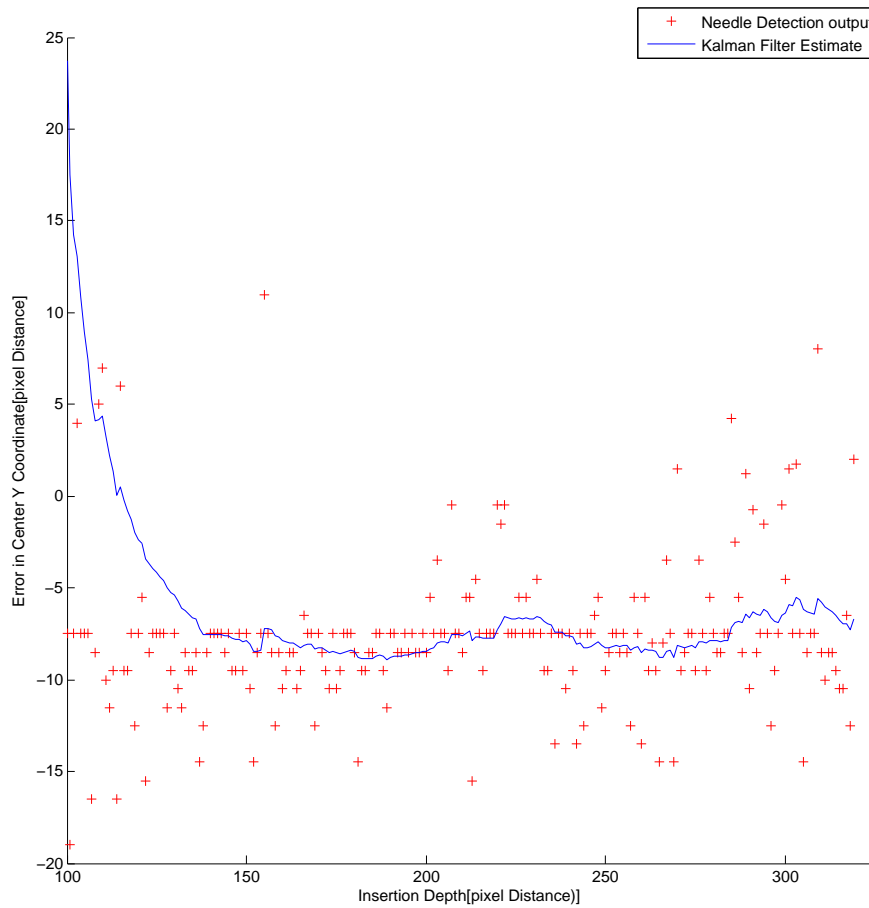


Figure 3.17: Deviation in b value in needle detection output and KF tracking from actual needle parameters for curved needle tracking. In the image the pixel spacing is 0.352mm

Figure 3.3.1 shows the deviation of detected and tracked values of radius of curvature R from actual needle parameters. The values represented in red are detected output from needle and the values represented in blue are output from KF tracking.

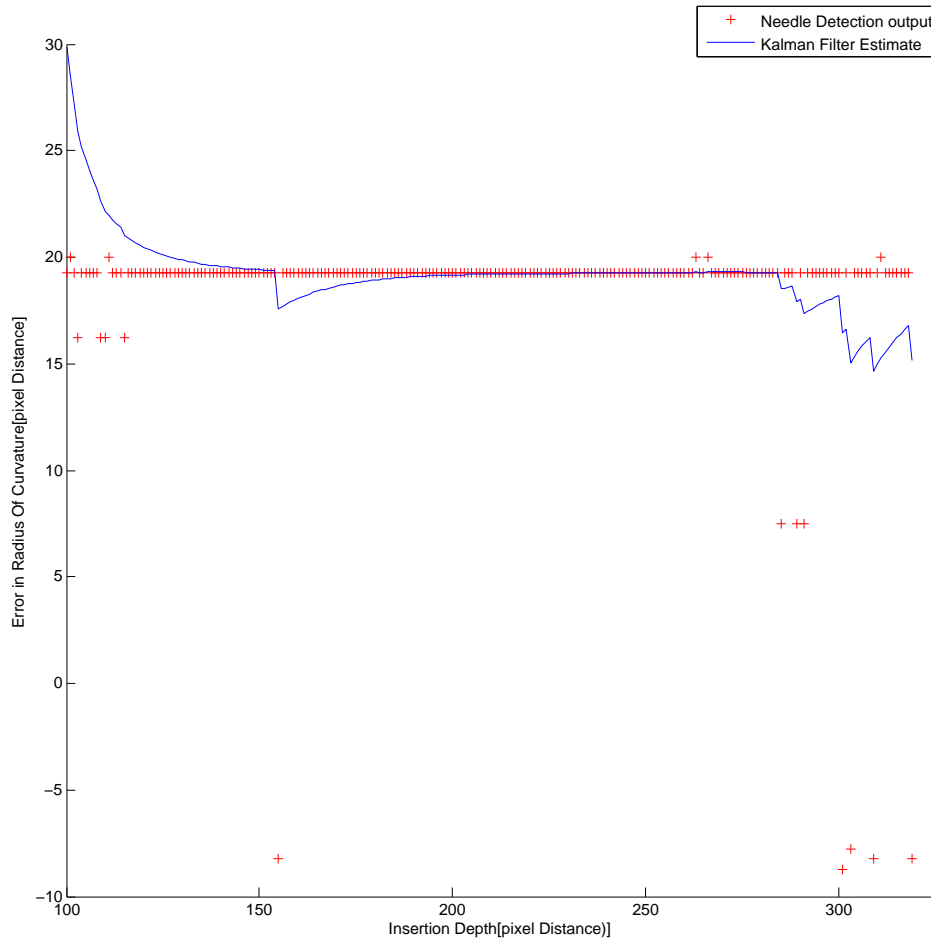


Figure 3.18: Deviation in r value in needle detection output and KF tracking from actual needle parameters for curved needle tracking. In the image the pixel spacing is 0.352mm

Figure 3.19 shows the time taken for needle tracking in each image. We can see that algorithm running time is increasing with the insertion depth because ROI also increases with insertion depth. Overall the algorithm runs less than 1.25s.

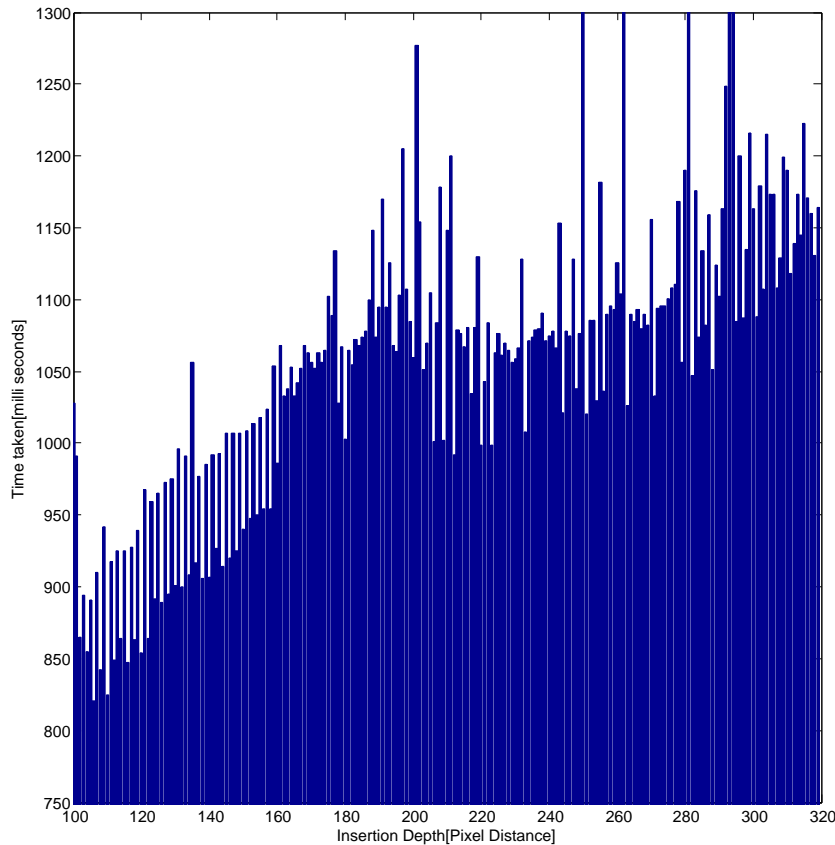


Figure 3.19: The time taken for needle tracking in the curved needle images

3.3.2 Experiments on real MRI data

As a substitute for biological tissue a soft Gelatin Phantom of size 100x100x200 mm using flavored Knox Gelatin(Knox gelatin, Kraft Foods Global Inc., Tarrytown, NY) was created. The gelatin was mixed at a ratio of 20 cc boiling water to 1.3 cc gelatin. This mixture has been proposed in the literature as an artificial tissue substitute for studies of this type. The gelatin was prepared in a vessel of 10x10x20 cm and an outer cannula needle

is fixed to the side of the bowl through a hole for inserting of inner needle.

Experiments were conducted on the images taken during the insertion of the needle into the gel phantom. The imaging was performed on a 3 Tesla MRI scanner (Philips Healthcare) deploying a Flex coil (Philips) and using a 2D T2WTSE sequence with $TR = 3000$ ms, $TE = 90$ ms, 218 kHz bandwidth, 1mm pixel spacing, 2 mm slice, 160x160 matrix. The needle we used is a pre-curved metallic needle of diameter 1.2mm. The frequency encoding direction and the static field were parallel to the needle shaft for in-plane images. Figure 3.20 shows a sample image and the needle detected in the image.

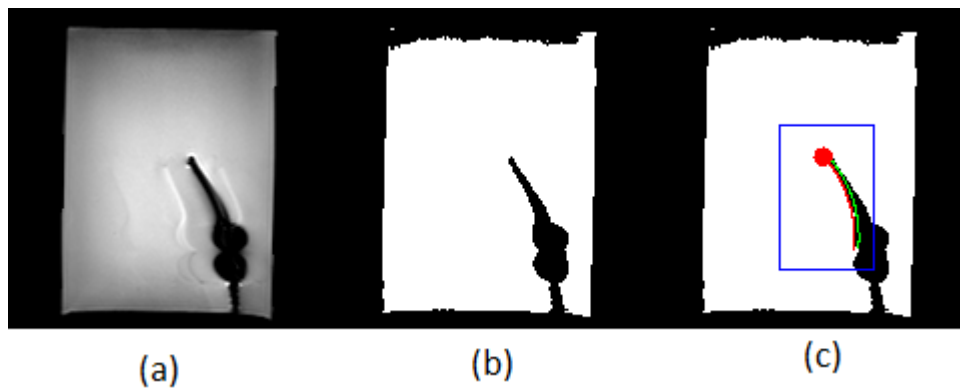


Figure 3.20: Curved Needle in Gelatin images :-a) Real MR image b) Thresholded Image c) Detected and Tracked needles

As we have used the pre-curved needle for this experiment, we know the radius of curvature for the surgical tool being inserted into the phantom. We analyze the detected parameters and Kalman Filter estimates of the needle parameters as the needle gets inserted into the phantom.

Figure 3.21 shows the detected and tracked values of X coordinate of the center of circular arc (a). The values represented in red are detected output from needle and the values represented in blue are output from KF tracking.

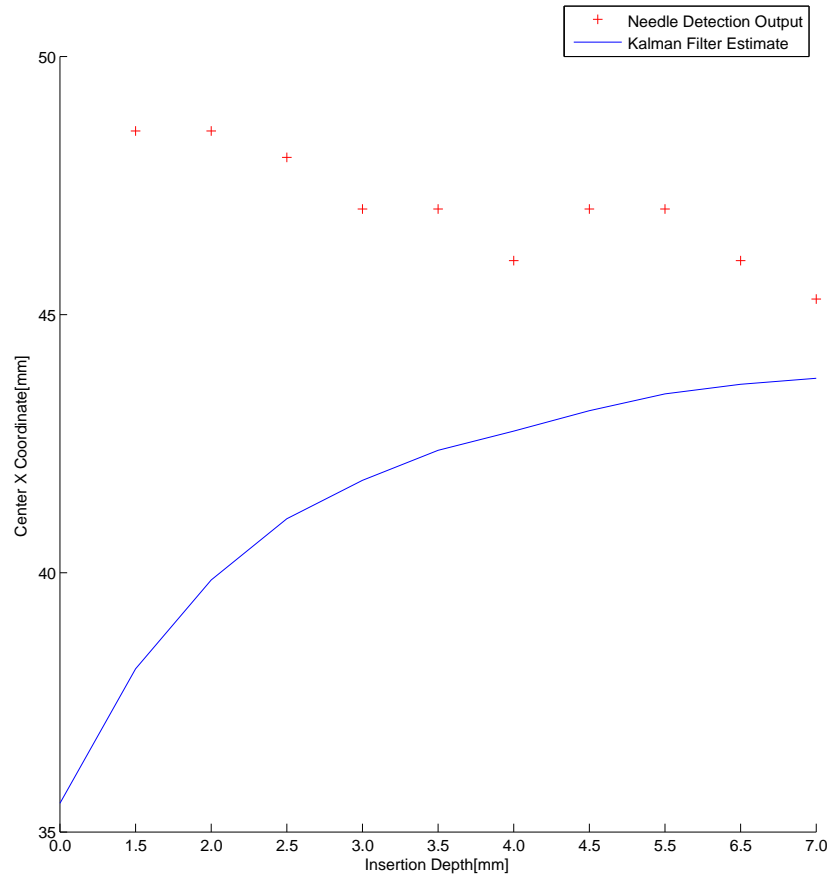


Figure 3.21: Curved Needle :- Tracked and detected values of Center X coordinate(a) for needle in the Gelatin images

Figure 3.22 shows the detected and tracked values of Y coordinate of the center of circular arc (b). The values represented in red are detected output from needle and the values represented in blue are output from KF tracking.

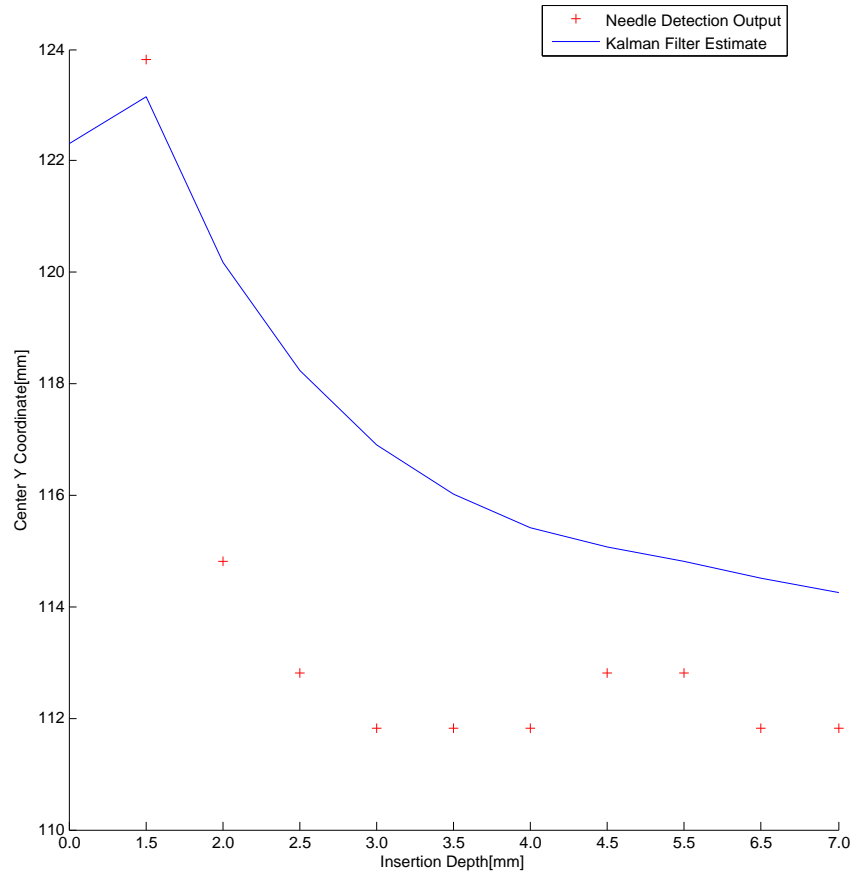


Figure 3.22: Curved Needle :-Tracked and detected values of Center Y coordinate(b) for needle in the Gelatin images

Figure 3.23 shows the detected and tracked values of radius of curvature (r) of circular arc. The values represented in red are detected output from needle and the values represented in blue are output from KF tracking. The actual curvature of the needle is represented in green.

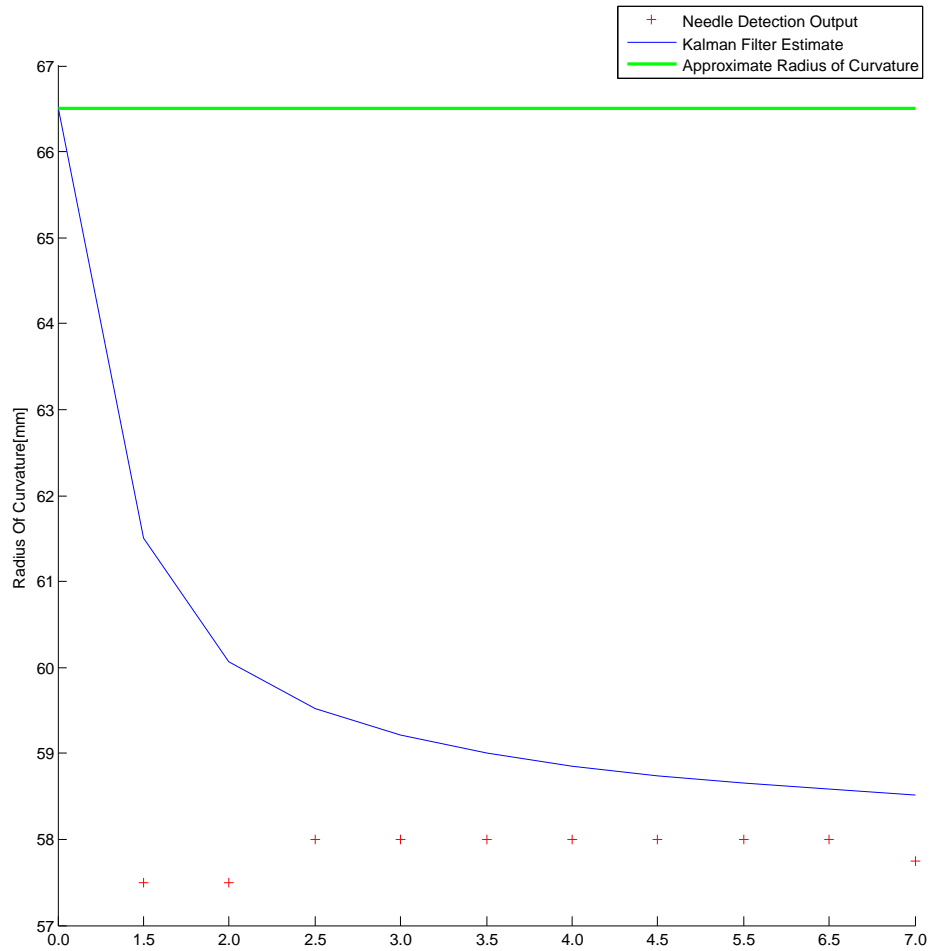


Figure 3.23: Curved Needle :- Tracked and detected values of Radius of Curvature for needle in the Gelatin images

3.4 Conclusion

The results show that the presented Hough-transform based image processing algorithm provides precise estimations of the current in-plane needle tip's position. Moreover, the proposed method can be integrated into a real application-like environment. The experiment in

the gel phantom allowed the application of the algorithm in a low noise and low disturbance environment. However, the artificial images created allowed us to simulate the tests with noisy, high resolution prostate real time MR images.

Furthermore, the results also show that the proposed method for tip location works, even if the tip is not visible in the needle artifact created. The results proved that the method allows an image update rate of one frame per second with a root mean squared error within 1.5 mm for straight needle and 2.5 mm for curved needle. The proposed method may therefore be feasible in MRI-guided targeted therapy such as prostate biopsies.

Chapter 4

Navigation Software

As shown in the Figure 4.1 the IGT system using surgical robots contains three main components i) MRI Scanner ii) Robot Controller Software and iii) Navigation Software. The communication between components happens through OpenIGTLink, a open source communication protocol developed for IGT purposes[34].

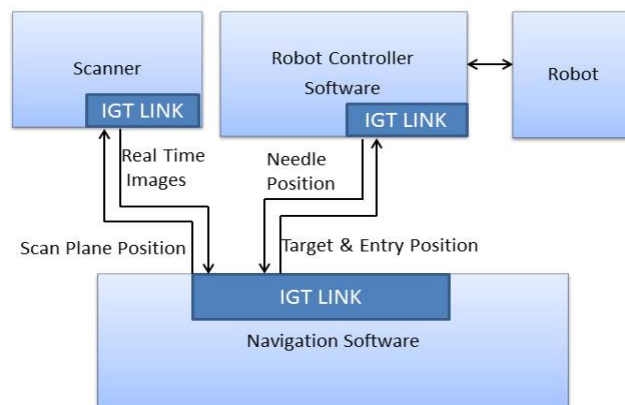


Figure 4.1: System architecture followed by AimLab, WPI for Image Guided Interventions using surgical robots

As an advancement towards having a full fledged image guided surgical systems using surgical robots, we have developed a Navigation software system that can be used in testing Image-guided procedures. We have also integrated the needle tracking approaches proposed in the software. The software is implemented in Java using Visualization Tool Kit(VTK) and Grassroots Dicom(GDCM). It has the following features.

Data Visualizaion :- Pre-operative MR images can be loaded and visualized in the navigation software as shown in Figure 4.2.

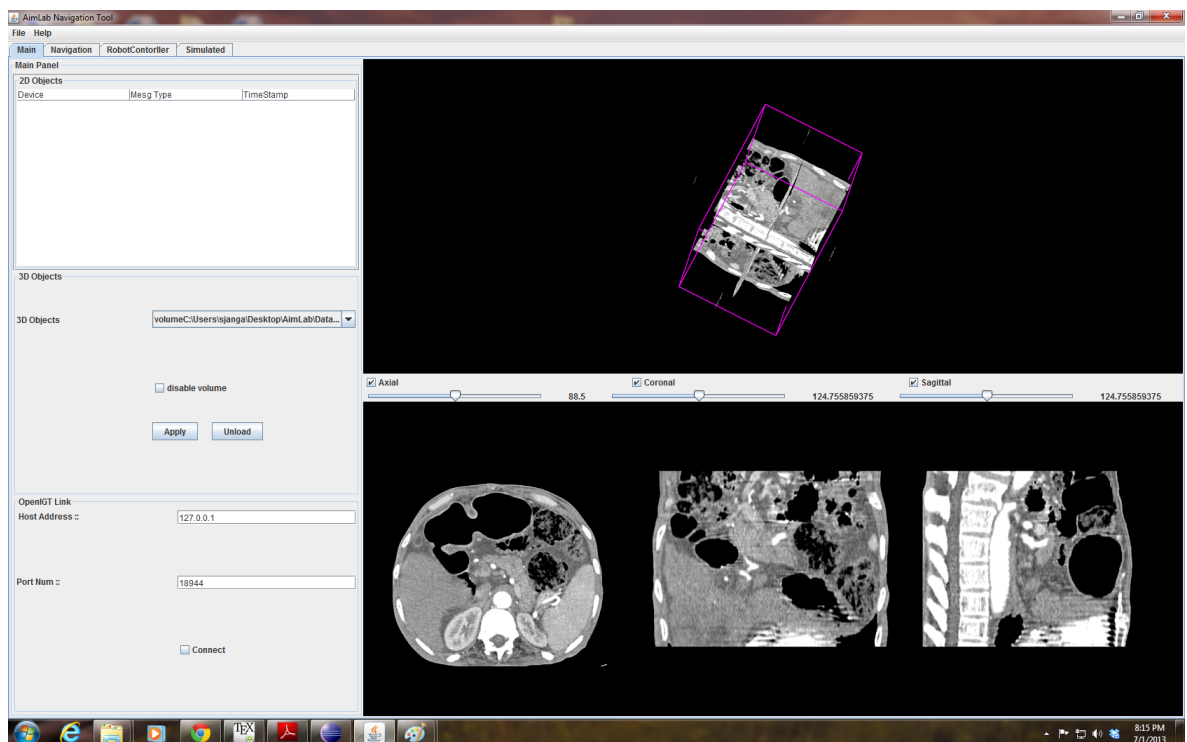


Figure 4.2: Displaying loaded volume

Surgical Planning and Guidance:- Surgeon can interactively select target and entry positions as shown in Figure 4.3. The navigation software does the path planning and transmits the position to robot controller through OpenIGTLink. The software can also receive the acquired real-time MR images during insertion and renders the surgical tool path as it navigates to the target.

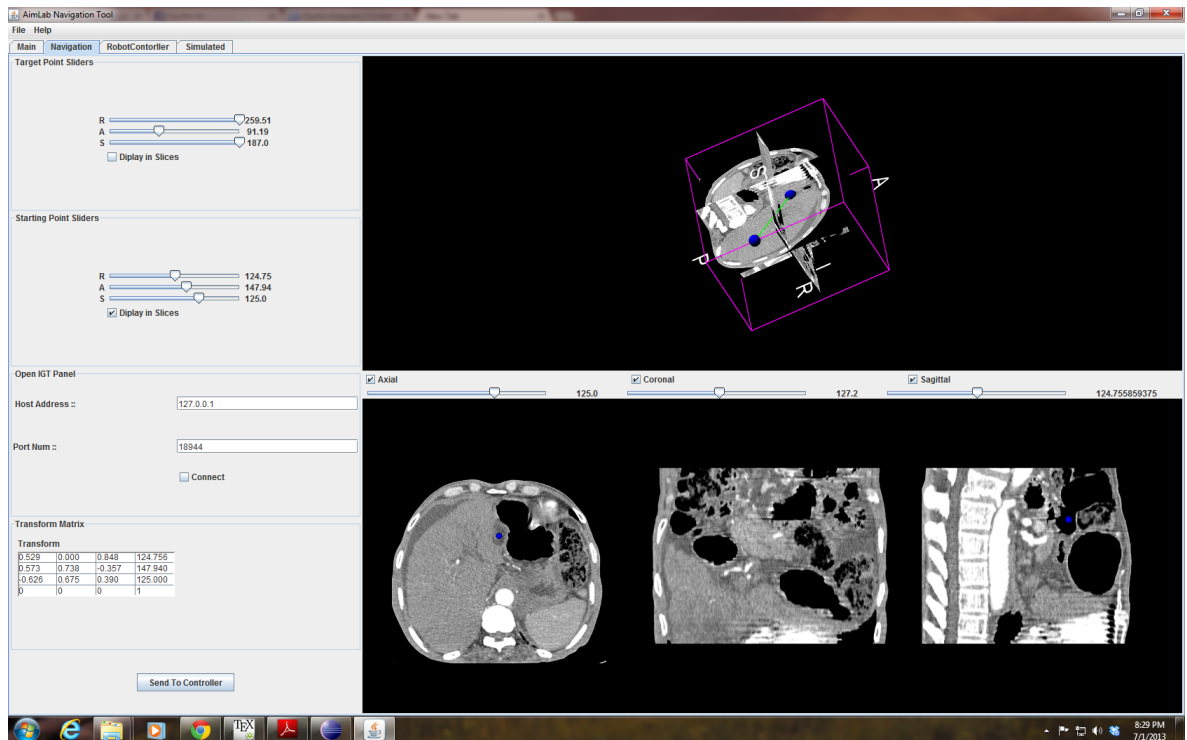


Figure 4.3: Displaying Selected Target and Entry Positions and the Path planned

Robot Control Software:- The robot control interface software shown in Figure 4.4 connects the Navigation software and the robot controller to exchange robot commands and coordinates using the OpenIGTLink. The targets or adjustments may also be directly entered or adjusted in the robot control interface software.

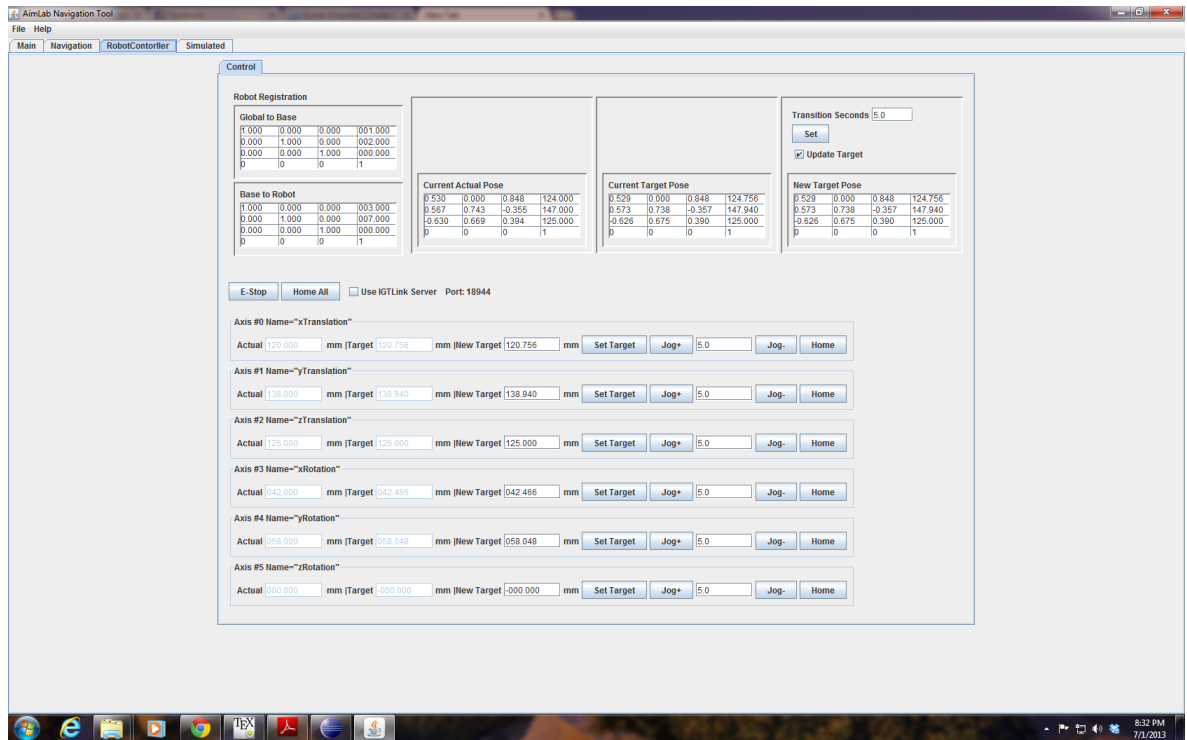


Figure 4.4: Robot Control Software for sending commands to robot controller

Virtual Robot:- As shown in the Figure 4.5 we have created a virtual robot that moves in sync with the real robot and help simulating the needle insertion. It receives commands through OpenIGTLink. This can be used for effective surgical planning and guidance.

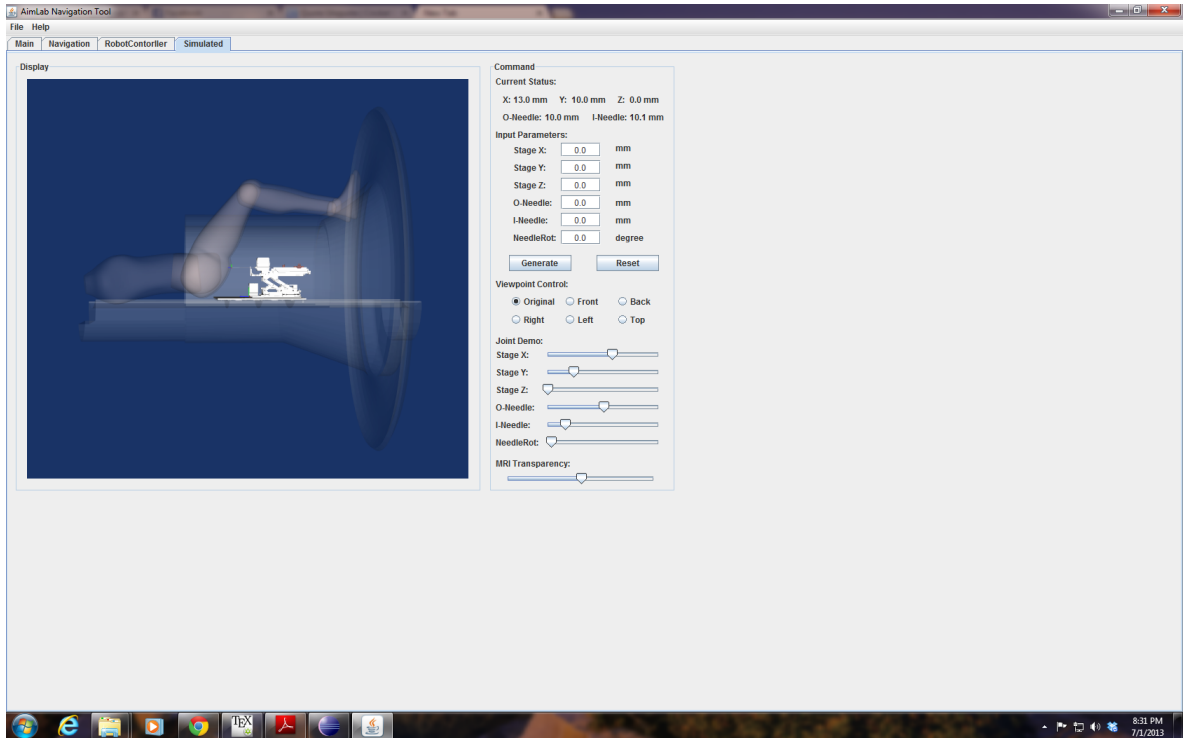


Figure 4.5: Virtual Robot used for Simulating needle insertion

Chapter 5

Future Work & Conclusions

Contribution:- This thesis dealt with the problem of automatic needle tracking in live imaging using external estimate information from robot and time series data with Kalman Filter.

The proposed methods are tested on 2D MR images of real data using the Gelatin Phantom and Simulated images. The proposed methods are fast enough to perform the needle tracking in real-time. By taking the result from needle tracking, the surgeons can visualize the the needle navigation on 2D/3D MRI. The proposed needle tracking method is fast and robust to needle bending even in the high resolution MR images. The proposed needle tip localization using parametrization of insertion depth is robust even if the tip is not visible in the needle artifact. The proposed method performs the needle tracking for a constant curved needles. We have shown in Chapter 3 that it can easily extended for tracking S-shape like needles.

Future Work:- More experiments with the real tissue should be performed to validate the proposed method in real clinical cases. We have done experiments with the phantom data, but other types of real tissues ex-vivo tissues should be also considered. Future research should also require comprehensive testing of the needle tracking approach on different gauges of needles. For some IGT applications it will be less invasive if multiply curved(for example an S- shape) are used. So we should extend and test this method for tracking the needle with multiple curved segments. Currently we are making assumptions about knowing the

2D plane where needle falls, this approach should be extended to tracking in 3D without making any assumptions.

Lessons Learned:- Considering its real-life applications needle-tracking is an important problem, that can make great contributions to the minimally invasive surgery. In the case of MRI, as needle does not output any signal, only highly noisy artifact can be seen in the image, which is mostly dark. To separate the needle object from the background is very challenging. None of the edge detection techniques like Canny [36] or Sobel [37] edge detector seemed to work due to presence of the gaps in the artifact and also needle is thin in the image. We also tried to fit many shape fitting approaches like Levenberg Marquardt [38] [39] least squares fitting and RANSAC fitting [30]. But they did not seem to work as the background vs foreground ratio is very high in MRI even after thresholding with needle intensity range.

Since MRI provides high resolution imaging, without knowing a-priori information about the needle position and axis, needle detection is really difficult even for the feature detectors like Hough Transform due to their high computational complexity.

Bibliography

- [1] T. Peters and K. Cleary, *Image Guided Interventions Technology and Applications*. ISBN 9780387738567, xxxii, 557, 2008.
- [2] G. Cole, J. Pilitsis, and G. S. Fischer., “Design of a robotic system for mri-guided deep brain stimulation electrode placement.,” in *Robotics and Automation ICRA '09*, pp. 4450-4456., 2009.
- [3] Y. Wang, G. A. Cole, H. Su, J. G. Pilitsis, and G. S. Fischer., “Mri compatibility evaluation of a piezoelectric actuator system for a neural interventional robot.,” in *Engineering in Medicine and Biology Society EMBC 2009*, pp. 6072-6075., 2009.
- [4] G. Cole, K. Harrington, H. Su, A. Camilo, J. Pilitsis, and G. Fischer., “Closedloop actuated surgical system utilizing real-time in-situ mri guidance.,” in *International Symposium on Experimental Robotics - ISER.*, 2010.
- [5] H. A. Paul, W. L. Bargar, B. Mittlestadt, B. Musits, R. H. Taylor, P. Kazanzides, J. Zuhars, B. Williamson, and W. Hanson., “Development of a surgical robot for cementless total hip arthroplasty.,” in *Clin Orthop Relat Res*, no. 285, pp. 57-66., 1992.
- [6] C. Rickers, M. Jerosch-Herold, X. Hu, N. Murthy, X. Wang, H. Kong, R. T. Seethamraju, J. Weil, and N. M. Wilke., “Magnetic resonance image-guided transcatheter closure of atrial septal defects.,” in *Circulation*, vol. 107, no. 1, pp. 132-138, 2003.
- [7] S. Xu, G. Fichtinger, R. H. Taylor, and K. R. Cleary., “3d motion tracking of pulmonary lesions using ct fluoroscopy images for robotically assisted lung biopsy.,” in

- Visualization, Image-Guided Procedures, and Display*, vol. 5367, no. 1, pp. 394-402., 2004.
- [8] G. S. Fischer, I. Iordachita, C. Csoma, J. Tokuda, P. W. Mewes, C. M. Tempany, N. Hata, and G. Fichtinger., “Pneumatically operated mri-compatible needle placement robot for prostate interventions.,” in *Robotics and Automation ICRA 2008*, pp. 2489-2495, 2008.
- [9] I. Rabi, J. Zacharias, S. Millman, and P. K. ., “A new method of measuring nuclear magnetic moment.,” in *Physical Review* 53 (4): 318327, 1938.
- [10] P. Lauterbur, “Image formation by induced local interactions: examples of employing nuclear magnetic resonance.,” in *Nature* 1973;242:1901, 1973.
- [11] A. Kumar, D. Welte, and R. Ernst, “Nmr fourier zeugmatography.,” in *J Mag Res* 1975;18:6983., 1975.
- [12] A. Garroway, P. Grannell, P. Mansfield, and J. Phys, “Image formation in nmr by a selective irradiative process.,” in *Solid State Phys* 1974;7:L45762, 1974.
- [13] H. Carr, “Free precession techniques in nuclear magnetic resonance.,” in *PhD thesis*, 1952.
- [14] M. Ding and A. Fenster, “A real-time biopsy needle segmentation technique using hough transform,” in *Med Physics*, Vol. 30, 2222-33, 2003.
- [15] Ding, M., Cardinal, H.N., and F. A., “Automatic needle segmentation in three-dimensional ultrasound images using two orthogonal two-dimensional image projections.,” in *Med Physics*, Vol. 30, 222-35., 2003.
- [16] R. A. Gorlitz, J. Tokuda, S. W. Hoge, R. Chu, L. P. Panych, C. Tempany, and N. Hata., “Development and validation of a real-time reduced field of view imaging driven by automated needle detection for mri-guided interventions.,” in *Visualization, Image-Guided Procedures, and Modelling*, Vol 7625., 2010.

- [17] P. V. C. Hough, "Method and means for recognizing complex patterns," in *U.S. Patent 3 069 654*, 1962.
- [18] R. O. Duda and P. E. Hart., "Use of the hough transformation to detect lines and curves in pictures.," in *Communications of Association for Computing Machinery*, 15(1):11-15., 1972.
- [19] D. H. Ballard, "Generalizing the hough transform to detect arbitrary shapes pattern recognition.," in 13(2):111-122., 1981.
- [20] D. Cyganski, W. F. Noel, and J. A., "The analytic hough transform .," in *Sensing and Reconstruction of Three-Dimensional Objects and Scenes.*, 1990.
- [21] L. Xu and E. Oja., "Randomized hough transform (rht): Basic mechanisms, algorithms, and computational complexities.," in *CVGIP: Image Understanding*, 57(2):131154., 1993.
- [22] L. Xu and E. Oja., "Randomized hough transform.," in *Encyclopedia of Artificial Intelligence*, pages 13541361., 2008.
- [23] L. Xu, E. Oja, and P. Kultanen., "A new curve detection method: randomized hough transform (rht).," in *Pattern Recognition Letters*, 11(5):331338., 1990.
- [24] H. Zhou, W. Qiu, M. Ding, and S. Zhang., "Automatic needle segmentation in 3d ultrasound images using 3d improved hough transform.," in *SPIE Medical Imaging.*, 2008.
- [25] N. Kiryati, Y. Eldar, and A. Bruckstein., "A probabilistic hough transform.," in *Pattern Recognition*, Volume 24, Issue 4, 1991, Pages 303-316, ISSN 0031-3203, DOI: 10.1016/0031-3203(91)90073-E., 1991.
- [26] H. Zhou, W. Qiu, and M. Ding., "Automatic needle segmentation in 3d ultrasound images using 3d hough transform.," in *SPIE Medical Imaging.*, 2007.
- [27] H. Zhou, W. Qiu, and M. Ding., "New realtime needle segmentation technique using grayscale hough transform.," in *SPIE Medical Imaging*, 2007.

- [28] K. S. Roberts., “A new representation for a line.,” in *CVPR, pages 635640.*, 1988.
- [29] P. Bhattacharya, H. Liu, A. Rosenfeld, and S. Thompson., “Hough-transform detection of lines in 3-d space.,” in *Pattern Recognition Letters, 21(9):843849.*, 2000.
- [30] M. A. Fischler and R. C. Bolles., “Random sample consensus: A paradigm for model fitting with applications to image analysis and automated cartography.,” in *CACM, 24(6):381395.*, 1981.
- [31] S. H. Okazawa, R. Ebrahimi, J. Chuang, R. N. Rohling, and S. E. Salcudean., “Methods for segmenting curved needles in ultrasound images.,”
- [32] M. Uhercik, J. Kybic, H. Liebgott, and C. Cachard., “Model fitting using ransac for surgical tool localization in 3d ultrasound images.,” in *IEEE Trans. of Biomedical Engineering*, 2009.
- [33] H. Ren, N. V. Vasilyev, and P. E. Dupont, “Detection of curved robots using 3d ultrasound.,” in *IROS.*, 2011.
- [34] J. Tokuda, G. Fischer, X. Papademetris, Z. Yaniv, L. Ibanez, P. Cheng, H. Liu, J. Blevins, J. Arata, A. Golby, T. Kapur, S. Pieper, E. Burdette, G. Fichtinger, C. Tempny, and N. Hata., “Openiglink: An open network protocol for image-guided therapy environment.,” in *The International Journal of Medical Robotics and Computer Assisted Surgery, Vol 5, No 4, pp 423-34.*, 2009.
- [35] R. Kalman, “A new approach to linear filtering and prediction problems.,” in *Journal of Basic Engineering 82 (1): 3545.*, 1960.
- [36] J. Canny, “A computational approach to edge detection.,” in *Pattern Analysis and Machine Intelligence, 8(6):679698*, 1986.
- [37] E. Davies, *Machine Vision: Theory, Algorithms and Practicalities.* Academic Press, 1990.
- [38] K. Levenberg, “A method for the solution of certain problems in least squares.,” in *Quart. Appl. Math. 2, 164-168*, 1944.

- [39] D. Marquardt, "An algorithm for least-squares estimation of nonlinear parameters.," in *SIAM J. Appl. Math.* 11, 431-441, 1963.